Discovery of calcium-metal alloy anodes for reversible Ca-ion batteries

Zhenpeng Yao,[12] Vinay I. Hegde,[2] Alán Aspuru-Guzik,[1345*] Chris Wolverton[2*]

[1]*Department of Chemistry and Chemical Biology, Harvard University, 12 Oxford Street, Cambridge, Massachusetts 02138, United States*

[2]*Department of Materials Science and Engineering, Northwestern University, 2220 Campus Drive, Evanston, Illinois 60208, United States*

[3]*Department of Chemistry and Department of Computer Science, University of Toronto, Toronto, Ontario M5S 3H6, Canada*

[4]*Vector Institute for Artificial Intelligence, Toronto, Ontario M5S 1M1, Canada*

[5]*Canadian Institute for Advanced Research (CIFAR) Senior Fellow, Toronto, Ontario M5S 1M1, Canada*

**Correspondence: alan@aspuru.com *Correspondence: c-wolverton@northwestern.edu*

Abstract

Ca-ion batteries (CIBs) show promise to achieve the high energy density required by emerging applications like electric vehicles because of their potentially improved capacities and high operating voltages. The development of CIBs has been hindered by the failure of traditional graphite and calcium metal anodes due to the intercalation difficulty and lacking efficient electrolyte. Recently a high voltage (4.45 V) CIB cell using Sn as the anode was reported achieving a remarkable cyclability (> 300 cycles). The calciation of Sn was observed to end at Ca_7Sn_6, which is surprising, since higher Ca-content compounds are known (*e.g.* Ca_2Sn). Here, we investigate computationally the Sn electrochemical calciation reaction process and explore the reaction

driving force as a function of Ca content using density functional theory (DFT) calculations. This exploration allows us to identify threshold voltages which govern the limits of the calciation process. We then use this information to design a four-step screening strategy and use high-throughput DFT to search for anode materials with higher properties. We predict that many metalloids (Si, Sb, Ge), (post-)transition metals (Al, Pb, Cu, Cd, $CdCu_2$) are promising inexpensive anode candidates and warrant further experimental investigations.

1. Introduction

The usage of renewable energy, coupled with the growing application of electric vehicles (EVs), demand energy storage techniques with high energy density and low cost.[1] Multivalent batteries, like Mg-ion,[2] Ca-ion,[3,4] and Al-ion batteries,[5,6] have the potential to realize significantly improved capacities, compared to monovalent batteries (*e.g.* Li-ion batteries), due to more electrons carried per ion. Among them, Ca-ion batteries (CIB) have drawn special attention with merits besides the capacity enhancement: 1) Ca/Ca^{2+} has a reduction potential (-2.87 V) only slightly higher than Li/Li^{+} (-3.04 V), yet much lower than Mg/Mg^{2+} (-2.36 V) and Al/Al^{3+} (-1.68 V), which provides CIB the prospect to function at voltages comparable with Li-ion batteries and much higher than the counterparts of Mg-ion and Al-ion batteries.[7,8] 2) Ca is the 5th most abundant element in the earth's crust with an extensive global resource distribution, in contrast to lithium. 3) The kinetics of Ca-ion in solid electrodes are faster than Mg- and Al-ions due to reduced charge density.[9–11]

The development of CIBs was originally pioneered by the study of Ca-ion electrochemical intercalations into layered transition metal oxides and sulfides.[12] Subsequently, many efforts then were made to search for cathode materials which will tolerate a large amount of Ca-ions reversibly extracted/re-accommodated upon charge/discharge. Material systems including Prussian blue

compounds,[10,13,14] Chevrel phases,[15,16] spinels,[17–19] perovskites,[20] layered transition metal (TM) sulfides,[21] and iron phosphate,[22] were suggested to be effective Ca-ion electrodes with the spinels and perovskites attracting extra attention because of their predicted high voltage (> 3.5V) and large theoretical capacities (> 240 mAh/g) during discharge at room temperature.[17–20] Distinct from these TM based electrodes, a graphite cathode has been reported which functions *via* the (de-)intercalation of electrolyte salt anions (A^- = PF_6^-, ClO_4^- and so on) upon charge/discharge at remarkably high voltages (5.2V)[23,24] with a theoretical capacity as high as 372 mAh/g (corresponding to AC_6).[25,26] Yet the practical capacity of batteries based on this material suffer from a large degradation (~90 mAh/g) as a result of the electrolyte decomposition under high voltage.[26]

Unlike the continuous development of CIB cathode materials, studies focusing on anodes have been relatively scarce. Graphite based CIB anodes have been shown to be problematic at room temperature due to difficulties related to the intercalation of calcium.[27] The pursuit of a calcium metal anode is currently hindered by the lack of an effective electrolyte to plate/strip calcium metal at room temperature[3] in an adequate voltage window.[4] Also, Ca^{2+} diffusion is observed to be extremely sluggish through the as-formed solid electrolyte interphase (SEI) between the calcium metal anode and the electrolyte.[28,29] TM oxide (*i.e.* V_2O_5)[30] based anodes have been shown to be effective at storing Ca-ions; however, the high calciation potential (~2.8 V) of this material significantly reduces the overall output voltage of the whole cell.[17]

Alloying-type anodes, widely studied for Li-ion batteries, show great promise for reversible CIBs. Using a Sn anode and graphite cathode, Wang *et al.*[14] recently reported a high voltage (4.45 V) CIB cell with a reasonable capacity of 85 mAh/g and a remarkable cyclability (95% capacity retention in 350 cycles). Besides Sn, several metals and metalloids including Zn,

Al, Si, Li, and Na also have been investigated for the use of alloying-type CIBs anodes with largely disparate capacities achieved.[13,14,31,32] All of them except Na have been reported to mix with Ca in wide composition ranges, forming various intermetallic compounds.[33] For instance, the highest Ca-content intermetallic compounds of Sn, Zn, and Li are Ca_2Sn,[34] Ca_3Zn[35] and $CaLi_2$,[36] with corresponding theoretical capacities calculated to be 903 mAh/g, 1366 mAh/g, and 3860 mAh/g. However, in experimental full cell operations, the calciation of Sn ends at Ca_7Sn_6 with a theoretical capacity of 527 mAh/g while the calciations of Zn and Li are even more truncated with very limited capacity observed.[14] It is therefore important to examine the metal-calcium (M-Ca) reaction mechanisms during the electrochemical calciation and understand the variation of the calciation driving force as a function of Ca-ions accommodated. Furthermore, considering that Ca mixes with many metals and metalloids, forming a wide range of alloys and compounds,[33] it is then of significant interest to explore the whole alloying space of M-Ca systems and discover novel active anode materials for improved electrochemical properties and cyclabilities.

First-principles density functional theory (DFT) calculations have been extensively used as compelling tools to study the battery materials by understanding the underlying mechanisms,[37–41] exploring the kinetics during electrochemical reactions,[42–45] and predicting novel high-performance electrode materials.[46–49] Here in this work, we use DFT to investigate the Sn-Ca electrochemical alloy reaction process *via* constructing the ground state Sn-Ca phase diagram and explore the reaction driving force evolution as a function of Ca-ion accommodated. We then identify the convex hull characteristics favored by large capacity alloy-type anodes and by comparison between our DFT calculations and electrochemical measurements of CIB cells, we define threshold calciation voltages which limit the extent of calciation reactions in real cells by examining the alloy reaction of Ca and Zn, Li, Na. Moreover, we design a four-step screening

strategy and use high-throughput DFT calculations to explore all M-Ca alloying space to search for anode materials with higher energy density and constrained volume expansion. We predict that many metalloids (Si, Sb, Ge), (post-)transition metals (Al, Pb, Cu, Cd, $CdCu_2$, Ga, Bi, In, Tl, Hg), and noble metals (Ag, Au, Pt, Pd) are promising anode candidates. Our discoveries shed light on the design of high performance reversible Ca-ion batteries and provide predictions of new compounds awaiting experimental validation.

2. Methodology

2.1 First-principles DFT calculations

All the first-principles calculations were performed *via* the Vienna Ab-initio Simulation Package (VASP)[50–53] within the projector augmented wave (PAW) formalism[54] and the Perdew-Becke-Ernzerhof (PBE) approximation[55] to the exchange-correlation potential was employed. We used a plane wave basis with a cutoff energy of 520 eV and **Γ**-centered *k*-meshes with a density of 8000 *k*-points per reciprocal atom. All the calculations reported in this study were conducted under the framework of the Open Quantum Materials Database (OQMD).[56,57]

2.2 Voltage profile calculations: calciation voltage and output voltage

2.2.1 Calciation voltage V of M-Ca anode

We evaluated the averaged M-Ca electrochemical alloy reaction voltages (calciation voltage, relative to Ca/Ca^{2+}) by calculating the reaction free energy per Ca added/removed, as shown in Eq. 1:[58,59]

$$V = \frac{\Delta G_{\mathrm{f}}}{2F\Delta N_{\mathrm{Ca}}} \quad (1)$$

where F is the Faraday constant, ΔN_{Ca} is the amount of Ca added/removed, 2 is the amount of charges carried per single Ca, and ΔG_{f} is the molar free energy change during the reaction.

Assuming that the calciation proceeds through a two-phase reaction between Ca_xM and M: $M + xCa \rightarrow Ca_xM$, ΔG_f can be approximated by the total internal energy changes from DFT calculations (0 K),

$$\Delta E = E(Ca_xM) - E(M) - xE(Ca_{metal}) \quad (2)$$

where $E(Ca_xM)$ and $E(M)$ are the DFT energies at the respective compositions. We neglected entropic contributions and the reaction voltage profiles therefore will follow the T = 0K ground state convex hull and consist of a series of constant voltage steps along the two-phase regions of the convex hull, separated by discontinuities indicating the single phase compounds on the hull. It is noteworthy that electrochemical M-Ca reactions do not necessarily proceed through two-phase reactions in practice. Thus, the calculated T = 0K voltage profiles should be viewed as an approximation to the actual voltage profiles.[60,61] The voltage drops in the profile become more rounded at finite temperatures (*e.g.*, room temperature), due to finite temperature effects.[59]

2.2.2 Output voltage V_{output} of CIBs using the M-Ca anode

During the discharge of CIBs, the M-Ca alloy anode, which is the focus of this study, experiences a decalciation reaction (corresponding voltage: $-V$) while the corresponding cathode experiences a calciation reaction (corresponding voltage: $V_{cathode}$). Upon charging, the reverse reactions occur. The output voltage of a complete CIB cell containing both cathode and anode upon discharge then can be defined as follows:

$$V_{output} = V_{cathode} - V \quad (4)$$

where the anode voltage V can be calculated using Eq. 1. To calculate the output voltage and then evaluate the energy densities of CIBs using anodes discovered in this study, we assume a value of $V_{cathode}$ = 5.2 V, consistent with the recent report of a graphite-based cathode material.[24]

We favor anodes with lower calciation voltage V to maximize the V_{output} of CIB, yet V should not be too low to ensure enough driving force for the reversed calciation reaction to happen on charge.

2.3 Volume expansion evaluations

We computed the volume expansion upon the calciation of M *via* calculating the volume change per Ca added as shown in Eq. 3:

$$U = \frac{u_{Ca_xM} - u_M}{x} \tag{3}$$

where $u_{\mathrm{Ca}_x\mathrm{M}}$ and u_{M} are the volumes of $\mathrm{Ca}_x\mathrm{M}$ and M respectively, x is the amount of Ca.

2.4 Capacity and energy density calculations

The gravimetric and volumetric capacity of M-Ca alloy anode corresponding to a given voltage plateau (a given two-phase reaction) can be calculated according to following equations Eq. 5 and Eq. 6:

$$C_g(V) = \frac{2\Delta N_{\mathrm{Ca}}(V)F}{m_M} \tag{5}$$

$$C_u(V) = \frac{2\Delta N_{\mathrm{Ca}}(V)F}{u_M} \tag{6}$$

where F is the Faraday constant, $\Delta N_{\mathrm{Ca}}(V)$ is the amount of Ca added/removed corresponding to the voltage plateau, 2 is the amount of charge carried per single Ca, m_M and u_M are the mass and volume of M, respectively.

The energy density $E_g(V)$ and specific energy $E_u(V)$ of the CIBs using the M-Ca alloy anode then can be calculated by integrating the volumetric capacity $C_g(V)$ and gravimetric capacity $C_u(V)$ as a function of output voltage V_{output} as shown in Eq. 7 and Eq. 8:

$$E_g(V) = \int_{V'}^{V_0} C_g(V_{cathode} - V')dV' \tag{7}$$

$$E_u(V) = \int_{V'}^{V_0} C_u(V_{cathode} - V')dV' \quad (8)$$

where V_0 is the lower limit of M calciation voltage profile.

3. Results and discussions

3.1 Sn-Ca phase diagram and the electrochemical Sn-Ca reactions

Phase diagrams represent the thermodynamic phase equilibria of multicomponent systems and provide useful information on the electrochemical reactions between phases. The ground state convex hull represents the T = 0 K limit of the thermodynamic phase diagram and gives information about the ground state stability of compounds in a given system. Experimental phase-diagram determination for a specific system can be time- and labor- consuming, while it can be significantly accelerated by calculating energies of all the known compounds in the corresponding chemical space using DFT.[47] Here we built M-Ca T = 0 K phase diagrams using structures with the lowest energy for each composition with M be metal/metalloids elements and their binary alloys. All the compounds were adopted from the Inorganic Crystal Structure Database (ICSD)[62] and corresponding calculations were carried out under the framework of OQMD.[56,57] Using these convex hulls, we analyze the electrochemical calciation process of Sn and examine the driving force variations to determine the calciation maximums for the Sn anode. Then we will validate our hypothesis in other typical systems including Zn, Li, and Na.

The calculated Sn-Ca convex hull is shown in Fig. 1A, we are able to correctly identify all the known intermediate phases in the experimental phase diagram including $CaSn_3$, CaSn, Ca_7Sn_6, $Ca_{31}Sn_{20}$, $Ca_{36}Sn_{23}$, and Ca_2Sn as either on the hull or slightly (< 10 meV/atom) above the hull.[34] The calciation voltages corresponding to these phases declines from 0.99 V, 0.72 V, 0.59 V, to 0.53 V relative to Ca/Ca^{2+} (Fig. 1B) while the volume expansions of the system per Ca accommodated increases from 7.4 $Å^3$, 27.5 $Å^3$, 27.6 $Å^3$, 28.8 $Å^3$, 31.1 $Å^3$ (Fig. 1C). By comparison

with experimental electrochemistry data, we can determine a cutoff for the allowed calciation driving force, below which the reaction will not proceed in practice. For instance, the experimental calciation of Sn ends at Ca_7Sn_6,[14] and the calculated calciation voltage of the Sn-Ca system (Fig. 1B) reaches a value of 0.53V (relative to Ca/Ca^{2+}) for Ca_7Sn_6. Hence, we use this comparison to hypothesize that the driving force for calciation of anodes should be no less than 0.53 V. We then validate the use this driving force limit to determine the calciation extent of Zn, Li, and Na (and other metals), and compare with experimental measurements below. We also note that the shape of the convex hull can have a profound impact on the extent of calciation. The Sn-Ca convex hull features a relatively steep decreasing energy on the Sn-rich side. The fast decrease in formation energy with increasing Ca content corresponds to high calciation voltages and a large reaction driving force while the "length" (in Ca content) of this segment of the convex hull indicates a large amount of Ca ions react with the anode when the driving force is large. On the contrary, convex hulls which feature short or shallow decreasing segments on the Ca-poor side indicate a weak driving force, or small Ca capacity, and potentially point to a hasty end to calciation.

3.2 Ca-Zn, Li, Na phase diagrams and the electrochemical calciation limits

Having determined a calciation voltage threshold in the Sn-Ca system, we next construct convex hulls in the Zn-Ca, Li-Ca, and Na-Ca systems, as shown in Fig. 2A. The DFT calculations show nearly all experimentally observed intermediate compounds on the hull (except $CaZn_3$ which we exclude because its reported crystal structure exhibits partial occupancies). Na is reported to show no solubility in Ca with no intermetallic compound reported. As a simple test of the immiscibility and lack of compound formation in this system, we used Li_2Ca as a prototype and calculate the corresponding Na_2Ca energy. The phase is above the hull, consistent with the lack of observed compounds in this system. The Zn-Ca convex hull is asymmetric with low energies on

the Zn-rich side, and formation energy of Ca_xZn rapidly decreases for small Ca concentrations ($0 < x < 0.33$). As a result, the calciation voltage quickly falls from 1.03 V to 0.46 V (Fig. 2B) in the same concentration range. If we apply the calciation voltage threshold derived from the Sn-Ca system (0.53V) to the Zn-Ca system, then we would predict its calciation should end at $x = 0.167$ ($CaZn_5$) and before $x = 0.33$ ($CaZn_2$), indicating a very limited calciation and capacity. These predictions are consistent with experimental observations,[14] thus validating the use of the calciation voltage threshold. Zn also exhibits a larger volume expansion per Ca of 31.26 $Å^3$ than Sn started at an early calciation step ($x = 0.167$) as shown in Fig. 2C. For the calciation reaction of Li, because the convex hull is extremely shallow with very small (negative) formation energies, and thus a low calciation voltage of 0.03 V (Fig. 2B). The Li-Ca calciation voltage is therefore significantly lower than the threshold calciation voltage value (0.53 V), and hence is predicted to exhibit very low reversible capacity, also in agreement with experimental observations,[14] and therefore validating the use of the threshold. For Na, no solubility in Ca and no stable intermediate phases, agrees with its poor calciation performance observed.[14] In order to obtain a significant calciation capacity, one should search for M-Ca convex hulls with long and fast decreasing segments to the M-rich side to ensure large capacity with a high driving force. Having validated our strategy, we next use our threshold calciation voltage combined with high-throughput (HT) DFT of a large number of alloying-type anode calciation reactions to discover novel anodes with promising electrochemical properties.

3.3 HT-DFT screening for high-performance novel calcium alloy anodes

Ca forms alloys with many metals and metalloids.[33] We use this fact, along with the threshold calciation voltage above to design a four-step screening strategy and apply it to search for the high electrochemical property anodes as shown in Fig. 3. The four steps are: (*i*) The

screening was initiated by identifying all the binary and ternary Ca intermetallic compounds from the Inorganic Crystal Structure Database (ICSD).[62] We exclude quaternary or higher order Ca alloys because of the potentially more complex mass transport (and hence sluggish kinetics) during their calciation and decalciation. In total, we identify unique 357 M-Ca compounds. (*ii*) We then examined all the Ca_xM compounds and checked the existence of counterparts with the same stoichiometry, but with Ca removed, *i.e.*, M. If both of them exist in the ICSD, the Ca_xM compound is then can be seen as the calciation product of M where this latter compound is either simply a metal/metalloid element (*e.g.* Sn) or a binary intermetallic compound $M_aM'_b$ (*e.g.* CuAu). This screen results in a pool of 115 M-Ca systems with a various number of calciation reactions. (*iii*) Next, we calculated calciation voltage profiles for calciation reactions of all 115 M-Ca systems as summarized in Fig. 4. To determine the practical extent of the calciation reactions of each M-Ca system and also its maximum capacity, we apply threshold calciation voltages to all the M-Ca systems. Two factors were considered to define the threshold calciation voltages: calcium metal plating and the practical calciation limit (discussed above). Anodes calciation potentials lower than Ca/Ca^{2+}, can experience calcium metal plating and possible dendrite formation, leading to possible short circuit and safety concerns. Therefore, we apply a first threshold calciation voltage of 0.1 V, which we term a "relaxed criterion", to avoid calcium plating and potential failure of the cell. Meanwhile, we also apply a second threshold calciation voltage of 0.53 V, obtained by determining the practical Sn calciation maximum as discussed above. The calciation driving force requirements for M-Ca systems could be different from Sn-Ca (although we validated this strategy above for Zn-Ca, Na-Ca, and Li-Ca systems), yielding some uncertainty in the predictions. Hence, we use both thresholds with 0.53 V serving as the restrictive criterion and the 0.1 V serving as the relaxed criterion. We repeated each screening calculation with both thresholds to illustrate the changes that

could occur with a range of calciation thresholds. Then two capacity maximums (C_{max}) of each M-Ca system are determined. (*iv*) For the two data sets obtained with different threshold calciation voltages, we estimated their output voltages refer to the $V_{cathode}$ assumed, volume expansions, specific energies, and energy densities and rank them using their maximum capacities and energy densities. Cyclabilities of alloying-type anodes are usually deteriorated by a large volume expansion due to ion insertions as we learned from the Li-ion batteries[63] and M-Ca systems with lower volume expansions are then favored. We then screen for M-Ca systems with a higher energy density than Sn, yielding a list of the most promising anode candidates.

3.3.1 Anode candidates obtained with the relaxed calciation voltage criterion

Metalloids (Si, Ge, As, Sb)

Our screening strategy identifies metalloids including Si, Ge, As, and Sb as compelling anode materials with high specific energies and remarkably constrained volume expansions as shown in Fig. 5. Among them, Si exhibits the highest gravimetric capacity (3817 mAh/g) and specific energy (18495 Wh/kg, calculated with graphite cathode usage assumed as discussed in Section 2.4) in this study by taking as many as 2 Ca. These attributes are significantly larger than the analogous properties of Sn (903 mAh/g, 4216 Wh/kg) when the lower threshold calciation voltage is applied. The average calciation voltage for the Si anode, 0.35V, is modest. Meanwhile, its maximum volume expansion is 31.89 $Å^3$ per Ca and is comparable to Sn (31.13 $Å^3$ per Ca). Ge, As and Sb also can take a maximum amount of 2 Ca per M when the low threshold calciation voltage was applied, and their heavier masses make their gravimetric capacities (1476 mAh/g, 1431 mAh/g, 880 mAh/g) and specific energies (6980 Wh/kg, 6371 Wh/kg, 3985 Wh/kg) slightly lower than Si, yet still comparable or higher than Sn. Moreover, Ge, As and Sb exhibit much lower volume expansion maximums than Sn: 31.06 $Å^3$, 30.93 $Å^3$, 29.66 $Å^3$ per Ca.

Post-transition metals (Ga, Al, In, Tl, Pb, Hg, Cd, Zn)

Post-transition metals contain candidates among which several have been investigated experimentally as anodes of CIBs such as Sn, Al, Zn. Boron-group metals including Ga, and Al exhibit attractive properties as alloy anodes for CIB because of their second and third highest specific energies (9746 Wh/kg, 9071 Wh/kg) predicted in this study (following Si) as well as outstanding gravimetric and volumetric capacities. Moreover, Al has a potentially low cost making it appealing for practical use in CIBs. The other two boron-group candidates (*i.e*. In and Tl) also can accommodate significant amounts of Ca (Ca_3In, Ca_3Tl) and exhibit high volumetric properties (Tab. 1) with volume expansions much lower than Ga and Al. Similar to In and Tl, Pb can accommodate 3 Ca per atom upon calciation with higher volumetric properties than Sn and the lowest volume expansion predicted in this study of 28.10 $Å^3$ per Ca, indicating the possibility of superior cycling performance than other candidates. Hg has been tried as liquid-state anode for CIB because of its low melting point, however, there are many intermetallic compounds in the Ca-Hg system that are stable at room temperature.[64] Thus to use Hg as an anode in a practical CIB, one could start with the lowest Ca-content compound of $CaHg_3$[64] and control the extent of decalciation to avoid the formation of liquid Hg metal. $CaHg_3$ has slightly lower gravimetric properties than Sn yet much higher volumetric capacity (7662 mAh/mL) and energy density (38923 Wh/L). Cd has been widely used in rechargeable NiCd batteries and here, we predict it to be a promising candidate for CIB with higher volumetric capacity (6227 mAh/mL) and energy density (30778 Wh/L) than Sn. Zn as an anode has been reported to fail[14] because of the rapid decreasing driving force in a very limited calciation concentration range.

Transition metal and alloys (Cu, $CdCu_2$)

Cu and $CdCu_2$ feature improved energy densities compared to Sn (5637 Wh/kg, 4249 Wh/kg). Meanwhile, Cu and its alloys have remarkable electrical conductivity which is a promising attribute for potential high-rate electrodes. In addition, their competitive costs which make them attractive for further experimental validations.

Noble metals (Pd, Au, Pt, Ag)

Noble metal candidates (Pd, Au, Pt) exhibit the highest volumetric capacities (18141 mAh/mL, 15830 mAh/mL, 14738 mAh/mL) and energy densities (88853 Wh/L, 77078 Wh/L, 69208 Wh/L) in this study by taking significant amount of Ca per metal (Ca_3Pd, Ca_3Au, Ca_5Pt_2). The calciation of Pd, Au, and Pt also occur at quite high calciation voltages for a large concentration range (Tab. S1) which ensure large reaction driving forces. Ag also shows improved volumetric properties compared to Sn at relatively lower potential (0.24V). Moreover, the noble metals' superior electrical conductivity and chemical stability against corrosion make them attractive candidates to be explored for CIB anodes. Their relatively high cost (except possibly Ag) may impair their large-scale applications yet their superb predicted properties make them worthy of scientific exploration.

3.3.2 Anode candidates obtained with the restrictive calciation voltage criterion

Metalloids (Si, As, Sb, Ge)

Metalloids are still the strongest anode candidates (Fig. 6) even with the strict calciation voltage threshold criterion and concomitant truncated calciation reaction (Tab. S1 and S2). Si, As, Sb and Ge exhibit highest gravimetric properties (gravimetric capacity: 1908 mAh/g, 1431 mAh/g, 880 mAh/g, 738 mAh/g; specific energy: 8874 Wh/kg, 6371 Wh/kg, 3985 Wh/kg, 3340 Wh/kg) which are significantly higher than Sn (527 mAh/g, 2426 Wh/kg) while Si and Ge also show competitive volume expansions (27.6 $Å^3$, 26.9 $Å^3$ per Ca) compared to Sn (27.59 $Å^3$ per Ca). Si

and Sb alloy-type anodes have also been extensively investigated in the Li-ion battery field, and their predicted properties suggest further experimental investigation of these anodes in CIB is warranted.

Post-transition metals (Bi)

Most post-transition metals which form alloys with Ca as discussed in the previous section experience lower calciation voltage compared with the restrictive voltage threshold. Bi emerges under the restrictive voltage threshold to be strong candidate CIB anode because of its comparable gravimetric properties with Sn yet much improved volumetric properties (5031 mAh/mL, 23206 Wh/L) and constrained volume expansion of 28.37 $Å^3$ per Ca.

Noble metals (Pt, Pd, Au)

The noble metals, Pd, Au, Pt, have relatively high calciation voltages over wide calciation reaction extents (Ca_5Pt_3, Ca_3Pd_2, Ca_5Au_3) and large energy densities (44498 Wh/L, 42259 Wh/L, 40824 Wh/L) with the strict criterion of 0.53 V. Their large volume expansions also get significantly relieved after the calciation reaction truncations (Tab. S2). Noble metals are still strong candidates for CIBs and scientific exploration.

4. Conclusions

In this study, we investigate the Sn-Ca electrochemical alloy reaction process *via* constructing the Sn-Ca T = 0K phase diagram and explore the reaction driving force evolution as a function of Ca-ion content accommodated. We identify the convex hull characteristics favored by large capacity alloy-type anodes which are then validated by Zn-Ca, Li-Ca, and Na-Ca systems and define threshold voltages to explain and determine the calciation reaction extent. Two threshold voltages are then put forward corresponding to the restrictive and relaxed criterions. The former threshold is based on the observed calciation behavior of Sn, and the latter threshold is

based on avoiding Ca metal plating and the possibility of dendrite formation. We design a four-step screening strategy based on voltage thresholds and use high-throughput DFT calculations to explore all M-Ca alloying spaces to search for anode materials with properties superior to the recently reported Sn anodes. We predict that many metalloids (Si, Sb, Ge), (post-)transition metals (Al, Pb, Cu, Cd, $CdCu_2$, Ga, Bi, In, Tl, Hg), and noble metals (Ag, Au, Pt, Pd) are promising anode candidates and worthy of further experimental validation. Our theoretical findings provide insights into the electrochemical calciation reaction process of alloy-type CIB anodes and could help in designing the reversible high-energy density CIB anode materials.

References

(1) Larcher, D.; Tarascon, J.-M. Towards Greener and More Sustainable Batteries for Electrical Energy Storage. *Nat. Chem.* **2015**, *7* (1), 19–29.

(2) Aurbach, D.; Lu, Z.; Schechter, A.; Gofer, Y.; Gizbar, H.; Turgeman, R.; Cohen, Y.; Moshkovich, M.; Levi, E. Prototype Systems for Rechargeable Magnesium Batteries. *Nature* **2000**, *407* (6805), 724–727.

(3) Ponrouch, A.; Frontera, C.; Bardé, F.; Palacín, M. R. Towards a Calcium-Based Rechargeable Battery. *Nat. Mater.* **2015**, *15* (2), 169–172.

(4) Wang, D.; Gao, X.; Chen, Y.; Jin, L.; Kuss, C.; Bruce, P. G. Plating and Stripping Calcium in an Organic Electrolyte. *Nat. Mater.* **2017**, *17* (1), 16–20.

(5) Lin, M.-C.; Gong, M.; Lu, B.; Wu, Y.; Wang, D.-Y.; Guan, M.; Angell, M.; Chen, C.; Yang, J.; Hwang, B.-J.; et al. An Ultrafast Rechargeable Aluminium-Ion Battery. *Nature* **2015**, *520* (7547), 324–328.

(6) Wang, D.-Y.; Wei, C.-Y.; Lin, M.-C.; Pan, C.-J.; Chou, H.-L.; Chen, H.-A.; Gong, M.; Wu, Y.; Yuan, C.; Angell, M.; et al. Advanced Rechargeable Aluminium Ion Battery with

a High-Quality Natural Graphite Cathode. *Nat. Commun.* **2017**, *8*, 14283–14289.

(7) Gummow, R. J.; Vamvounis, G.; Kannan, M. B.; He, Y. Calcium-Ion Batteries: Current State-of-the-Art and Future Perspectives. *Adv. Mater.* **2018**, 1801702.

(8) Ponrouch, A.; Palacin, M. R. On the Road toward Calcium-Based Batteries. *Curr. Opin. Electrochem.* **2018**.

(9) Nightingale, E. R. Phenomenological Theory of Ion Solvation. Effective Radii of Hydrated Ions. *J. Phys. Chem.* **1959**, *63* (9), 1381–1387.

(10) Gheytani, S.; Liang, Y.; Wu, F.; Jing, Y.; Dong, H.; Rao, K. K.; Chi, X.; Fang, F.; Yao, Y. An Aqueous Ca-Ion Battery. *Adv. Sci.* **2017**, *4* (12), 1700465–1700471.

(11) Muldoon, J.; Bucur, C. B.; Gregory, T. Quest for Nonaqueous Multivalent Secondary Batteries: Magnesium and Beyond. *Chem. Rev.* **2014**, *114* (23), 11683–11720.

(12) Whittingham, M. S. Chemistry of Intercalation Compounds: Metal Guests in Chalcogenide Hosts. *Prog. Solid State Chem.* **1978**, *12* (1), 41–99.

(13) Lipson, A. L.; Pan, B.; Lapidus, S. H.; Liao, C.; Vaughey, J. T.; Ingram, B. J. Rechargeable Ca-Ion Batteries: A New Energy Storage System. *Chem. Mater.* **2015**, *27* (24), 8442–8447.

(14) Wang, M.; Jiang, C.; Zhang, S.; Song, X.; Tang, Y.; Cheng, H.-M. Reversible Calcium Alloying Enables a Practical Room-Temperature Rechargeable Calcium-Ion Battery with a High Discharge Voltage. *Nat. Chem.* **2018**, *10* (6), 667–672.

(15) Smeu, M.; Hossain, M. S.; Wang, Z.; Timoshevskii, V.; Bevan, K. H.; Zaghib, K. Theoretical Investigation of Chevrel Phase Materials for Cathodes Accommodating Ca2+ Ions. *J. Power Sources* **2016**, *306*, 431–436.

(16) Rogosic, J. Towards the Development of Calcium Ion Batteries, Massachusetts Institute of

Technology, 2014.

(17) Cabello, M.; Nacimiento, F.; González, J. R.; Ortiz, G.; Alcántara, R.; Lavela, P.; Pérez-Vicente, C.; Tirado, J. L. Advancing towards a Veritable Calcium-Ion Battery: CaCo2O4 Positive Electrode Material. *Electrochem. commun.* **2016**, *67*, 59–64.

(18) Dompablo, M. E. A.; Krich, C.; Nava-Avendaño, J.; Biškup, N.; Palacín, M. R.; Bardé, F. A Joint Computational and Experimental Evaluation of CaMn2O4 Polymorphs as Cathode Materials for Ca Ion Batteries. *Chem. Mater.* **2016**, *28* (19), 6886–6893.

(19) Liu, M.; Rong, Z.; Malik, R.; Canepa, P.; Jain, A.; Ceder, G.; Persson, K. A. Spinel Compounds as Multivalent Battery Cathodes: A Systematic Evaluation Based on Ab Initio Calculations. *Energy Environ. Sci.* **2015**, *8* (3), 964–974.

(20) Arroyo-de Dompablo, M. E.; Krich, C.; Nava-Avendaño, J.; Palacín, M. R.; Bardé, F. In Quest of Cathode Materials for Ca Ion Batteries: The CaMO3 Perovskites (M = Mo, Cr, Mn, Fe, Co, and Ni). *Phys. Chem. Chem. Phys.* **2016**, *18* (29), 19966–19972.

(21) Tchitchekova, D. S.; Ponrouch, A.; Verrelli, R.; Broux, T.; Frontera, C.; Sorrentino, A.; Bardé, F.; Biskup, N.; Arroyo-de Dompablo, M. E.; Palacín, M. R. Electrochemical Intercalation of Calcium and Magnesium in TiS2: Fundamental Studies Related to Multivalent Battery Applications. *Chem. Mater.* **2018**, *30* (3), 847–856.

(22) Lipson, A. L.; Kim, S.; Pan, B.; Liao, C.; Fister, T. T.; Ingram, B. J. Calcium Intercalation into Layered Fluorinated Sodium Iron Phosphate. *J. Power Sources* **2017**, *369*, 133–137.

(23) Carlin, R. T.; Long, H. C. De; Fuller, J.; Trulove, P. C. Dual Intercalating Molten Electrolyte Batteries. *J. Electrochem. Soc.* **1994**, *141* (7), L73–L76.

(24) Read, J. A.; Cresce, A. V.; Ervin, M. H.; Xu, K. Dual-Graphite Chemistry Enabled by a High Voltage Electrolyte. *Energy Environ. Sci.* **2014**, *7* (2), 617–620.

(25) Billaud, D.; Pron, A.; Lincoln Vogel, F. Electrical Resistivity and X-Ray Spacings of Graphite Tetrafluoroborate, Hexafluorophosphate and Hexafluoroantimonate Compounds Synthesized from Nitronium Salts. *Synth. Met.* **1980**, *2* (3–4), 177–184.

(26) Seel, J. A.; Dahn, J. R. Electrochemical Intercalation of PF6- into Graphite. *J. Electrochem. Soc.* **2000**, *147* (3), 892–898.

(27) Emery, N.; Hérold, C.; Lagrange, P. Structural Study and Crystal Chemistry of the First Stage Calcium Graphite Intercalation Compound. *J. Solid State Chem.* **2005**, *178* (9), 2947–2952.

(28) Tchitchekova, D. S.; Monti, D.; Johansson, P.; Bardé, F.; Randon-Vitanova, A.; Palacín, M. R.; Ponrouch, A. On the Reliability of Half-Cell Tests for Monovalent (Li+, Na+) and Divalent (Mg2+, Ca2+) Cation Based Batteries. *J. Electrochem. Soc.* **2017**, *164* (7), A1384–A1392.

(29) Aurbach, D.; Skaletsky, R.; Gofer, Y. The Electrochemical Behavior of Calcium Electrodes in a Few Organic Electrolytes. *J. Electrochem. Soc.* **1991**, *138* (12), 3536–3545.

(30) Amatucci, G. G.; Badway, F.; Singhal, A.; Beaudoin, B.; Skandan, G.; Bowmer, T.; Plitz, I.; Pereira, N.; Chapman, T.; Jaworski, R. Investigation of Yttrium and Polyvalent Ion Intercalation into Nanocrystalline Vanadium Oxide. *J. Electrochem. Soc.* **2001**, *148* (8), A940–A950.

(31) Tran, T. T.; Obrovac, M. N. Alloy Negative Electrodes for High Energy Density Metal-Ion Cells. *J. Electrochem. Soc.* **2011**, *158* (12), A1411–A1416.

(32) Ponrouch, A.; Tchitchekova, D.; Frontera, C.; Bardé, F.; Dompablo, M. E. A.; Palacín, M. R. Assessing Si-Based Anodes for Ca-Ion Batteries: Electrochemical Decalciation of

CaSi2. *Electrochem. commun.* **2016**, *66*, 75–78.

(33) Vrana, L. M. Calcium and Calcium Alloys. In *Kirk-Othmer Encyclopedia of Chemical Technology*; John Wiley & Sons, Inc.: Hoboken, NJ, USA, 2011; pp 1–10.

(34) Palenzona, A.; Manfrinetti, P.; Fornasini, M. . Phase Diagram of the Ca–Sn System. *J. Alloys Compd.* **2000**, *312* (1–2), 165–171.

(35) Okamoto, H. Ca-Zn (Calcium-Zinc). *J. Phase Equilibria Diffus.* **2013**, *34* (2), 171–171.

(36) Franke, P.; Neuschütz, D.; (SGTE), S. G. T. E. Ca-Li (Calcium - Lithium). In *Binary Systems. Part 5: Binary Systems Supplement 1*; Springer Berlin Heidelberg: Berlin, Heidelberg; pp 1–3.

(37) Kang, K.; Meng, Y. S.; Bréger, J.; Grey, C. P.; Ceder, G.; Ceder, G. Electrodes with High Power and High Capacity for Rechargeable Lithium Batteries. *Science (80-.).* **2006**, *311* (5763), 977–980.

(38) Yao, Z.; Kim, S.; Aykol, M.; Li, Q.; Wu, J.; He, J.; Wolverton, C. Revealing the Conversion Mechanism of Transition Metal Oxide Electrodes during Lithiation from First-Principles. *Chem. Mater.* **2017**, *29* (21), 9011–9022.

(39) Zhan, C.; Yao, Z.; Lu, J.; Ma, L.; Maroni, V. A.; Li, L.; Lee, E.; Alp, E. E.; Wu, T.; Wen, J.; et al. Enabling the High Capacity of Lithium-Rich Anti-Fluorite Lithium Iron Oxide by Simultaneous Anionic and Cationic Redox. *Nat. Energy* **2017**, *2* (12), 963–971.

(40) Li, Q.; Liu, H.; Yao, Z.; Cheng, J.; Li, T.; Li, Y.; Wolverton, C.; Wu, J.; Dravid, V. P. Electrochemistry of Selenium with Sodium and Lithium: Kinetics and Reaction Mechanism. *ACS Nano* **2016**, *10* (9), 8788–8795.

(41) Urban, A.; Seo, D.-H.; Ceder, G. Computational Understanding of Li-Ion Batteries. *npj Comput. Mater.* **2016**, *2* (1), 16002–16014.

(42) Morgan, D.; Van der Ven, A.; Ceder, G. Li Conductivity in LixMPO4 (M = Mn, Fe, Co, Ni) Olivine Materials. *Electrochem. Solid-State Lett.* **2004**, *7* (2), A30–A32.

(43) Yao, Z.; Kim, S.; Michel, K.; Zhang, Y.; Aykol, M.; Wolverton, C. Stability and Conductivity of Cation and Anion Substituted LiBH4-Based Solid-State Electrolytes. *Phys. Rev. Mater.* **2018**, *2* (6), 065402–065408.

(44) Yu, H.-C.; Ling, C.; Bhattacharya, J.; Thomas, J. C.; Thornton, K.; Van der Ven, A. Designing the next Generation High Capacity Battery Electrodes. *Energy Environ. Sci.* **2014**, *7* (5), 1760–1768.

(45) Rong, Z.; Malik, R.; Canepa, P.; Sai Gautam, G.; Liu, M.; Jain, A.; Persson, K.; Ceder, G. Materials Design Rules for Multivalent Ion Mobility in Intercalation Structures. *Chem. Mater.* **2015**, *27* (17), 6016–6021.

(46) Jain, A.; Hautier, G.; Moore, C. J.; Ping Ong, S.; Fischer, C. C.; Mueller, T.; Persson, K. A.; Ceder, G. A High-Throughput Infrastructure for Density Functional Theory Calculations. *Comput. Mater. Sci.* **2011**, *50* (8), 2295–2310.

(47) Yao, Z.; Kim, S.; He, J.; Hegde, V. I.; Wolverton, C. Interplay of Cation and Anion Redox in Li4Mn2O5 Cathode Material and Prediction of Improved Li4(Mn,M)2O5 Electrodes for Li-Ion Batteries. *Sci. Adv.* **2018**, *4* (5), eaao6754.

(48) Curtarolo, S.; Hart, G. L. W.; Nardelli, M. B.; Mingo, N.; Sanvito, S.; Levy, O. The High-Throughput Highway to Computational Materials Design. *Nat. Mater.* **2013**, *12* (3), 191–201.

(49) Amsler, M.; Yao, Z.; Wolverton, C. Cubine, a Quasi Two-Dimensional Copper–Bismuth Nanosheet. *Chem. Mater.* **2017**, *29* (22), 9819–9828.

(50) Kresse, G.; Hafner, J. Ab Initio Molecular Dynamics for Liquid Metals. *Phys. Rev. B*

1993, *47*, 558–561.

(51) Kresse, G.; Hafner, J. Ab Initio Molecular-Dynamics Simulation of the Liquid-Metal-Amorphous-Semiconductor Transition in Germanium. *Phys. Rev. B* **1994**, *49* (20), 14251–14269.

(52) Kresse, G.; Furthmüller, J. Efficiency of Ab-Initio Total Energy Calculations for Metals and Semiconductors Using a Plane-Wave Basis Set. *Comput. Mater. Sci.* **1996**, *6*, 15–50.

(53) Kresse, G. Efficient Iterative Schemes for Ab Initio Total-Energy Calculations Using a Plane-Wave Basis Set. *Phys. Rev. B* **1996**, *54* (16), 11169–11186.

(54) Blöchl, P. E. Projector Augmented-Wave Method. *Phys. Rev. B* **1994**, *50* (24), 17953–17979.

(55) Perdew, J. P.; Ernzerhof, M.; Burke, K. Rationale for Mixing Exact Exchange with Density Functional Approximations. *J. Chem. Phys.* **1996**, *105* (22), 9982–9985.

(56) Kirklin, S.; Saal, J. E.; Meredig, B.; Thompson, A.; Doak, J. W.; Aykol, M.; Rühl, S.; Wolverton, C. The Open Quantum Materials Database (OQMD): Assessing the Accuracy of DFT Formation Energies. *npj Comput. Mater.* **2015**, *1*, 15010–15024.

(57) Saal, J. E.; Kirklin, S.; Aykol, M.; Meredig, B.; Wolverton, C. Materials Design and Discovery with High-Throughput Density Functional Theory: The Open Quantum Materials Database (OQMD). *JOM* **2013**, *65* (11), 1501–1509.

(58) Aydinol, M. K.; Kohan, A. F.; Ceder, G.; Cho, K.; Joannopoulos, J. Ab Initio Study of Lithium Intercalation in Metal Oxides and Metal Dichalcogenides. *Phys. Rev. B* **1997**, *56* (3), 1354–1365.

(59) Wolverton, C.; Zunger, A. First-Principles Prediction of Vacancy Order-Disorder and Intercalation Battery Voltages in LixCoO2. *Phys. Rev. Lett.* **1998**, *81* (3), 606–609.

(60) Liu, H.; Li, Q.; Yao, Z.; Li, L.; Li, Y.; Wolverton, C.; Hersam, M. C.; Dravid, V. P. Origin of Fracture-Resistance to Large Volume Change in Cu-Substituted Co3O4 Electrodes. *Adv. Mater.* **2017**, *30* (4), 1704851–1704858.

(61) Li, Q.; Wu, J.; Yao, Z.; Thackeray, M. M.; Wolverton, C.; Dravid, V. P. Dynamic Imaging of Metastable Reaction Pathways in Lithiated Metal Oxide Electrodes. *Nano Energy* **2017**, *44*, 15–22.

(62) Belsky, A.; Hellenbrandt, M.; Karen, V. L.; Luksch, P. New Developments in the Inorganic Crystal Structure Database (ICSD): Accessibility in Support of Materials Research and Design. *Acta Crystallogr. Sect. B Struct. Sci.* **2002**, *58* (3), 364–369.

(63) Beaulieu, L. Y.; Eberman, K. W.; Turner, R. L.; Krause, L. J.; Dahn, J. R. Colossal Reversible Volume Changes in Lithium Alloys. *Electrochem. Solid-State Lett.* **2001**, *4* (9), A137–A140.

(64) Guminski, C. The Ca-Hg (Calcium-Mercury) System. *J. Phase Equilibria* **1993**, *14* (1), 90–96.

Acknowledgement

Funding: Z.Y. (Conceived the idea, DFT calculations, and analysis of results) and A.A.-G. (leadership of project) were supported as part of the Nanoporous Materials Genome Center by the U.S. Department of Energy, Office of Science, Office of Basic Energy Sciences under award number DE-SC0008688. C.W. (leadership of project) was supported as part of the Center for Electrochemical Energy Science (CEES), an Energy Frontier Research Center funded by the U.S. Department of Energy, Office of the Science, Basic Energy Science under the award number DE-AC02-06CH11357. V.I.H. (high-throughput workflows) acknowledges support from the Center

for Hierarchical Materials Design (CHiMaD) and from the U.S. Department of Commerce, National Institute of Standards and Technology under award no. 70NANB14H012. We gratefully acknowledge the computing resources from: 1) the National Energy Research Scientific Computing Center, a DOE Office of Science User Facility supported by the Office of Science of the U.S. Department of Energy under Contract DE-AC02-05CH11231. 2) Blues, a high-performance computing cluster operated by the Laboratory Computing Resource Center at Argonne National Laboratory. **Author contributions:** Z.Y. conceived the overall project and DFT calculation of ground state structure prediction, structural pathway, voltage and energy density. C.W. provided overall direction and advice for project, and analyzed the results. V.I.H. performed high-throughput calculation of doping options. A.A-G. provided feedback for the project. **Competing interests:** All authors declare that they have no competing interests. **Data and materials availability:** All data needed to evaluate the conclusions in the paper are present in the paper and/or the Supplementary Materials. Additional data related to this paper may be requested from the authors.

Figures

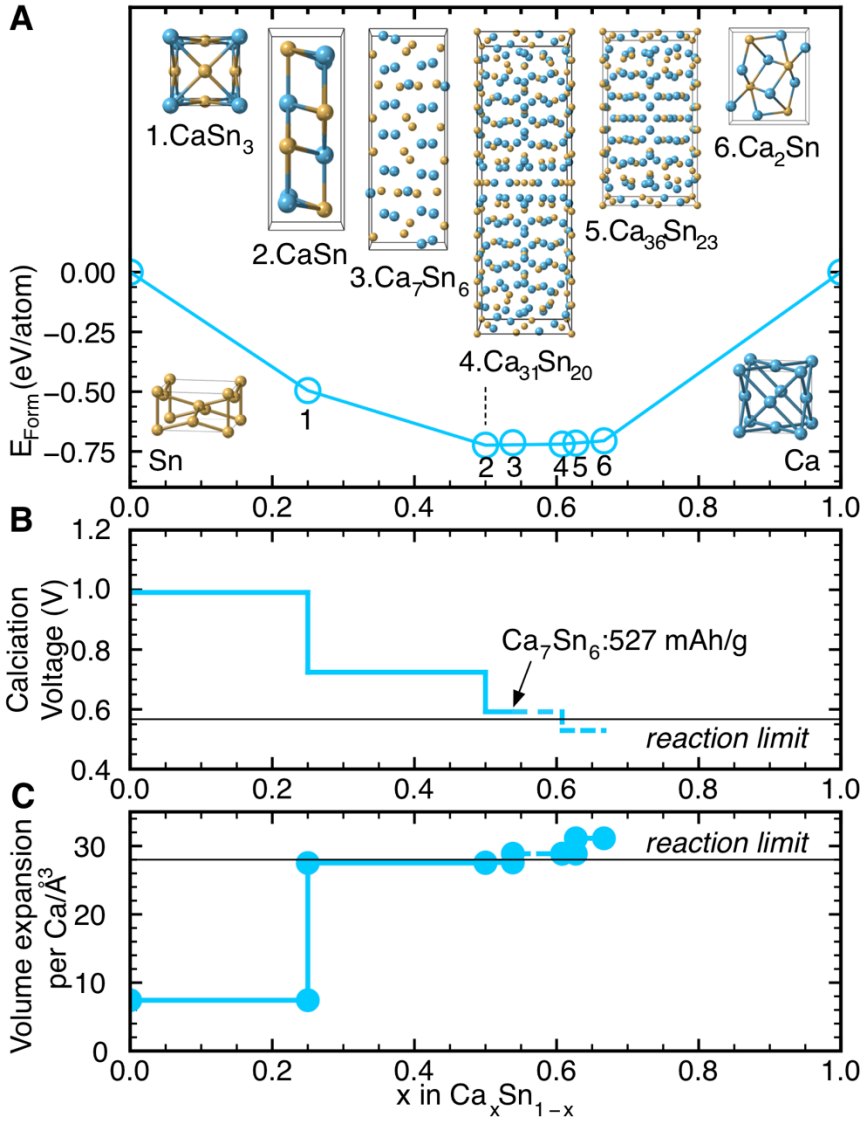

Figure 1. Electrochemical calciation process of Sn. (A) Sn-Ca convex hull with all the known Sn-Ca intermetallic compounds predicted to be on or slightly (< 10 meV/atom) above the convex hull. Structures for Sn, Ca, and all the intermetallic compound are shown in the insets. (B) Corresponding calciation voltage profile during the calciation process of Sn. Experimentally observed calciation ends at Ca_7Sn_6 before the calciation voltage profile reaching the last plateau of 0.53 V,[14] which can be seen as the threshold voltage of calciation. (C) Calculated volume expansion per Ca as a function of calciation.

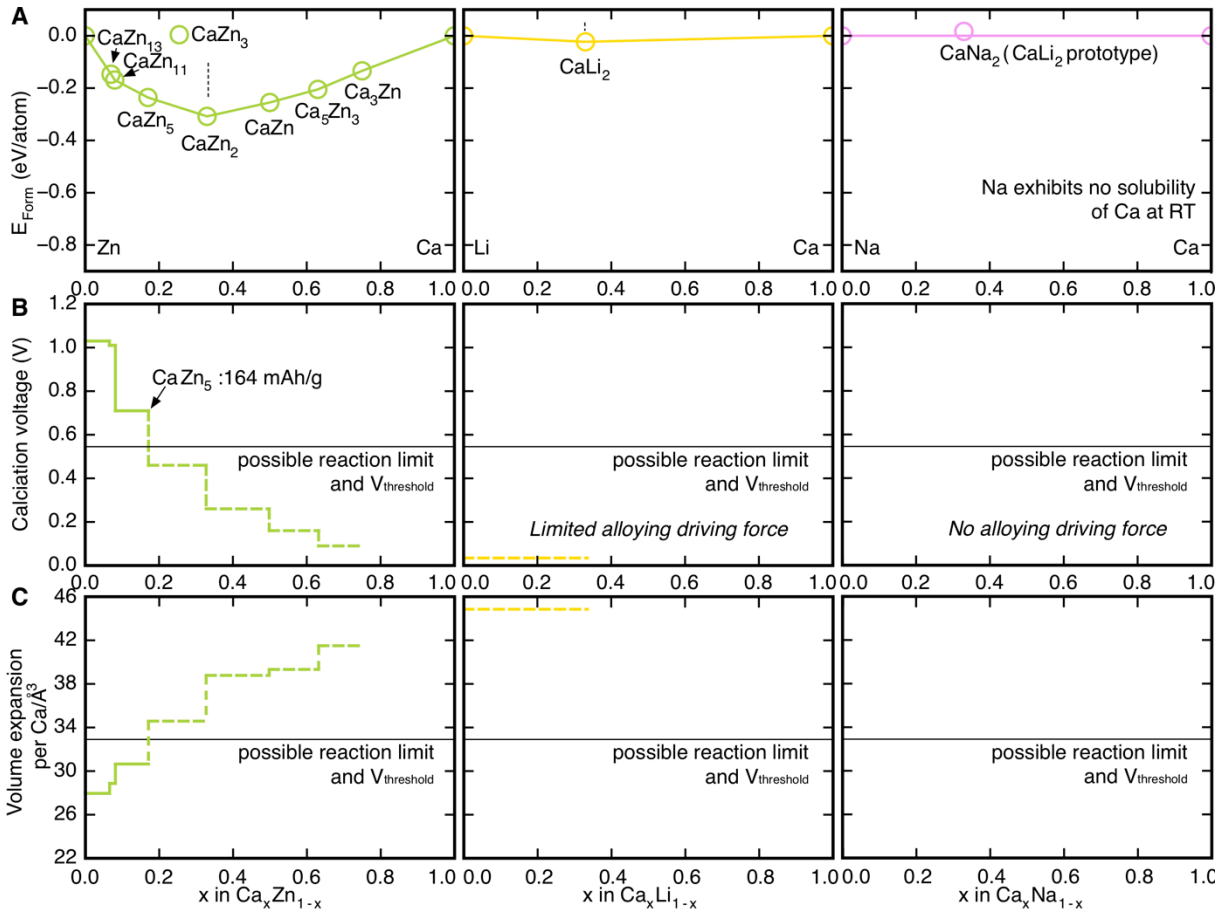

Figure 2. Electrochemical calciation processes of Zn, Li, Na and the determination of M-Ca alloy anode calciation threshold voltage. (A) Zn-Ca, Li-Ca, Na-Ca convex hulls. (B) Corresponding calciation voltage profiles during the calciation of Zn and Li. (C) Calculated volume expansions per Ca upon calciations of Zn and Li. Compare with the Sn-Ca convex hull, the bottom of the Zn-Ca convex hull deviated to the Zn side with rapidly decreased formation energy in a small Ca concentration range indicating a fast calciation voltage declining and losing of reaction driving force. Similarly, the extremely shallow feature of the Li-Ca convex hull implying a low calciation voltage and inadequate reaction driving force, validating the observed significantly limited calciation capacity of Zn and Li.[14] No stable intermetallic compound is identified for the Na-Ca convex hull, reflecting the fact of no solubility of Ca in Na.

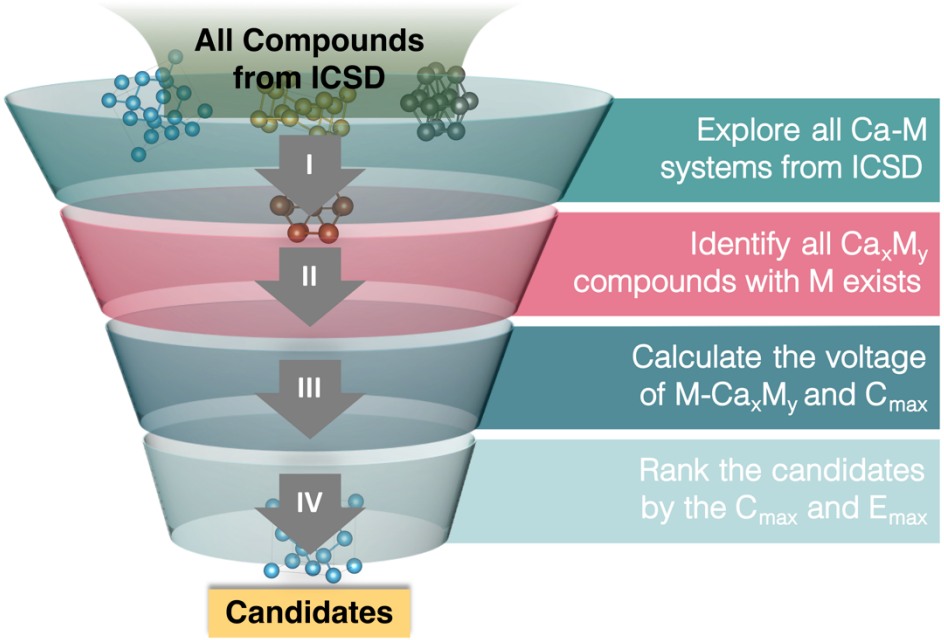

Figure 3. Screening strategy for the search of calcium-metal alloy anodes. We proceeded the high-throughput screening following a four-step strategy. Started with all the compounds in the Inorganic Crystal Structure Database (ICSD), we identify the M-Ca alloys for which the M also exists in the ICSD with M can be metal elements and other alloys. Then we calculate the reaction voltage profiles for each M-Ca system and determine its maximum capacity C_{max}. Lastly, we evaluate the energy densities E_{max} corresponding to C_{max} of all the systems using their output voltage, rank them based on their E_{max} values, and select the ones with highest energy densities as our top candidates.

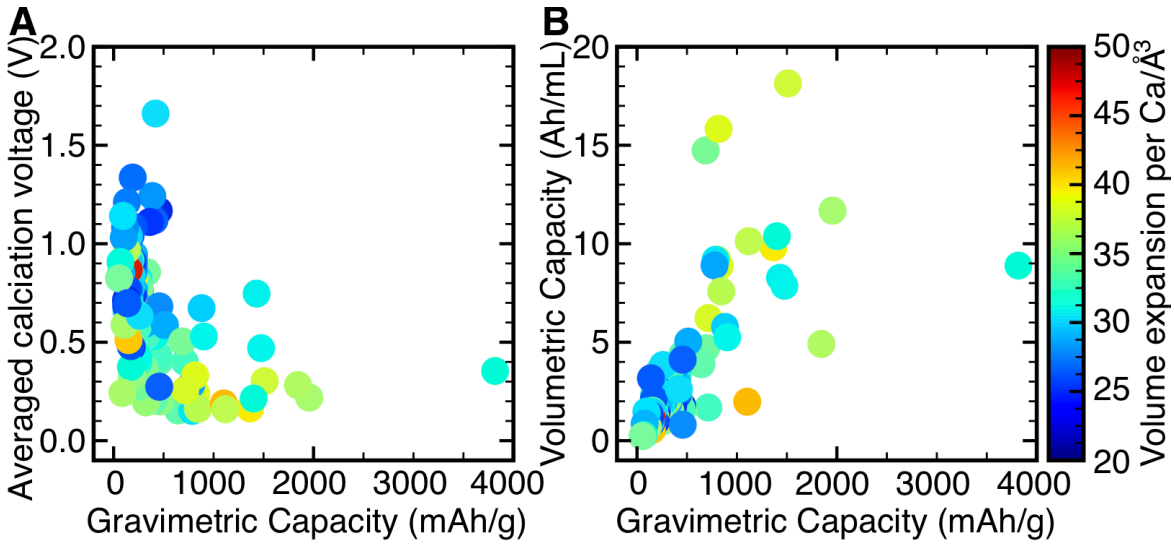

Figure 4. Summary of the identified M-Ca systems and corresponding properties. (A) Averaged calciation voltages and gravimetric capacities and (B) Volumetric capacities of all the 115 M-Ca systems. The color of each marker indicates the volume expansion per Ca corresponding to the final product of specific M-Ca system.

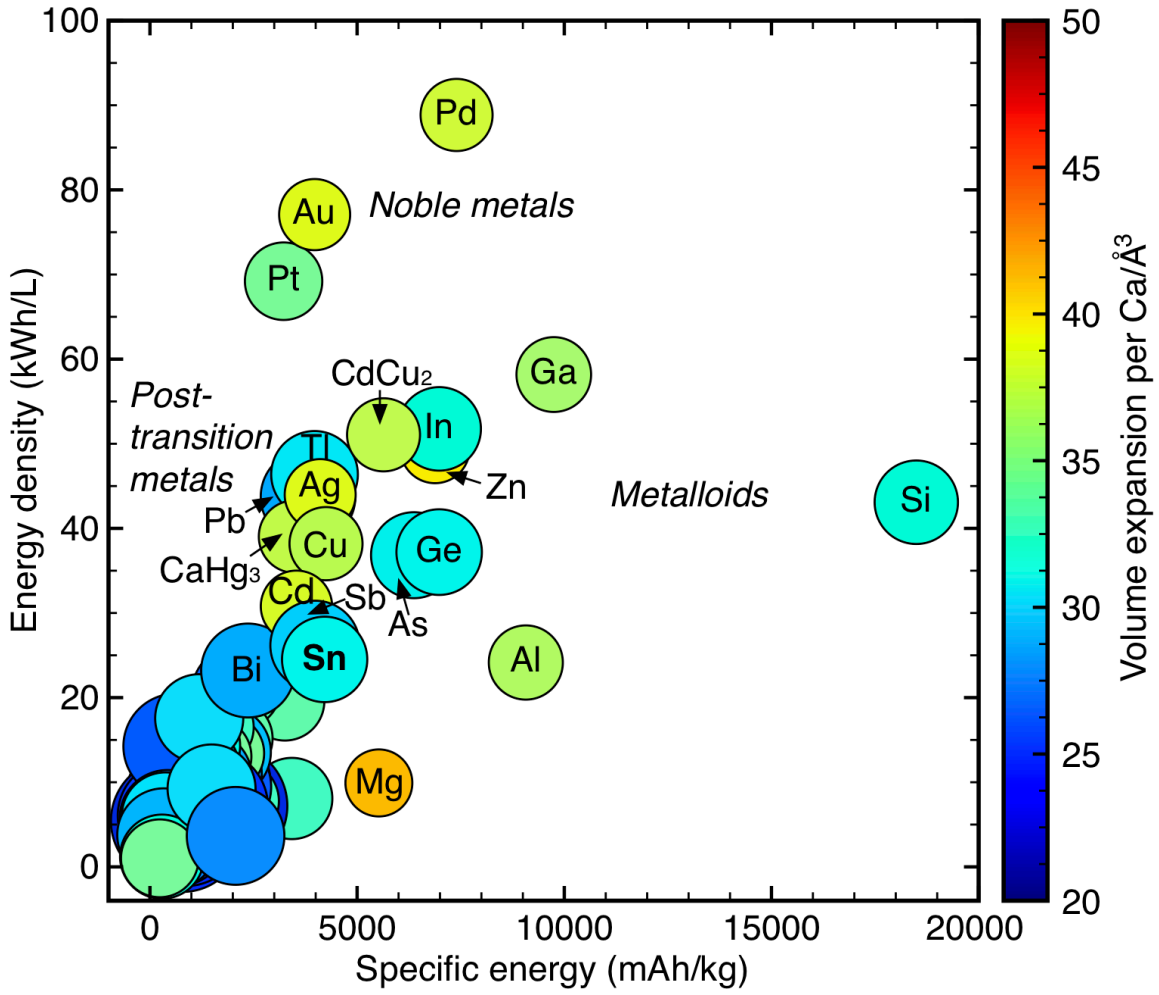

Figure 5. HT-DFT screening results for high performance M-Ca anodes with relaxed voltage constraint. We performed computational screening for M-Ca alloy-type anode materials. Candidates are systems with energy densities and specific energies (calculated with graphite cathode usage assumed as discussed in Section 2.4) higher than the counterparts of Sn. The color (and size) of each marker indicates the volume expansion (inversed trend for size) per Ca. Our top candidates are metalloids (Si, Ge, As, Sb), post-transition metals (Ga, Al, In, Tl, Pb, Hg, Cd), transition metals (Cu, $CdCu_2$), and noble metals (Pd, Au, Pt, Ag).

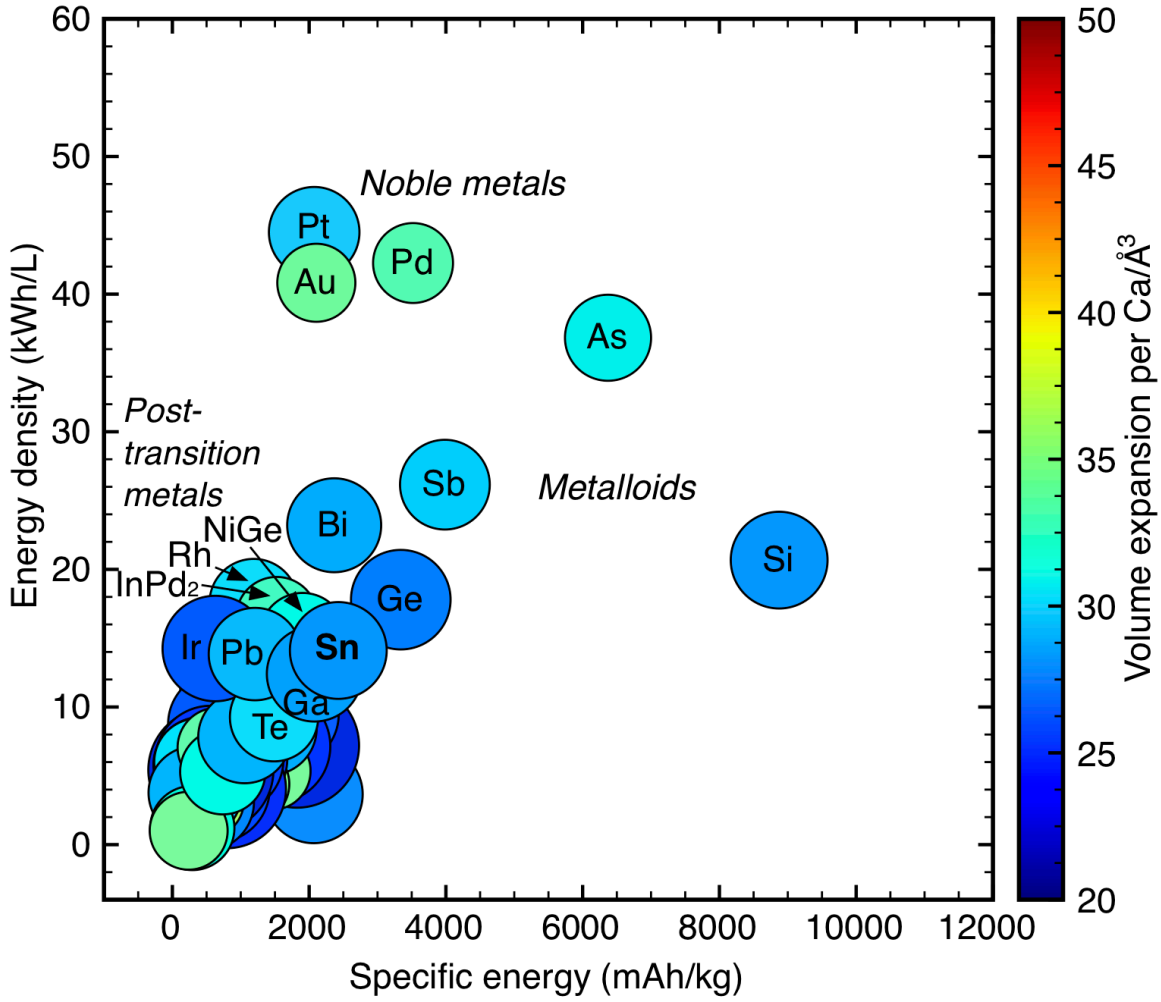

Figure 6. HT-DFT screening results for high performance M-Ca anodes with restrictive voltage constraint. We performed computational screening for M-Ca alloy-type anode materials. Candidates are systems with energy densities and specific energies (calculated with graphite cathode usage assumed as discussed in Section 2.4) higher than the counterparts of Sn. The color (and size) of each marker indicates the volume expansion (inversed trend for size) per Ca. Our top candidates are metalloids (Si, As, Sb, Ge), post-transition metals (Bi), and noble metals (Pt, Pd, Au).

Table 1. Candidates for high performance M-Ca alloy-type anodes with relaxed voltage constraint ($V_{threshold}$ = 0.1V). For each candidate system we show the reactant, final product, averaged voltage, gravimetric capacity, volumetric capacity, energy density, specific energy, and volume expansion maximum.

Candidates and reactions	Averaged calciation voltage (V)	Gravimetric Capacity (mAh/g)	Volumetric Capacity (mAh/mL)	Energy Density (Wh/L)	Specific Energy (Wh/kg)	Volume Expansion per Ca/Å^3
$Si + 2Ca \rightarrow Ca_2Si$	0.35	3817	8892	43089	18495	31.89
$Ga + 28/11Ca \rightarrow 1/11Ca_{28}Ga_{11}$	0.22	1957	11680	58178	9746	36.12
$Al + 13/14Ca \rightarrow 1/14Ca_{13}Al_{14}$	0.28	1845	4910	24149	9071	36.47
$Pd + 3Ca \rightarrow Ca_3Pd$	0.30	1511	18141	88853	7400	37.75
$In + 3Ca \rightarrow Ca_3In$	0.21	1400	10381	51759	6982	31.89
$Ge + 2Ca \rightarrow Ca_2Ge$	0.47	1476	7864	37195	6980	31.06
$Zn + 5/3Ca \rightarrow 1/3Ca_5Zn_3$	0.16	1366	9816	49435	6881	39.78
$As + 2Ca \rightarrow Ca_2As$	0.75	1431	8271	36830	6371	30.93
$CdCu_2 + 5Ca \rightarrow Ca_5CdCu_2$	0.16	1119	10130	51056	5637	37.14
$Cu + Ca \rightarrow CaCu$	0.16	843	7581	38192	4249	37.10
$Ag + 5/3Ca \rightarrow 1/3Ca_5Ag_3$	0.24	828	8866	43982	4108	38.47
$Sb + 2Ca \rightarrow Ca_2Sb$	0.67	880	5778	26156	3985	29.66
$Au + 3Ca \rightarrow Ca_3Au$	0.33	816	15830	77078	3975	38.42
$Tl + 3Ca \rightarrow Ca_3Tl$	0.15	787	9185	46373	3972	30.62
$Pb + 3Ca \rightarrow Ca_3Pb$	0.28	776	8897	43744	3816	28.10
$Cd + 3/2Ca \rightarrow 1/2Ca_3Cd_2$	0.26	715	6227	30788	3536	38.22
$Pt + 5/2Ca \rightarrow 1/2Ca_5Pt_2$	0.50	687	14738	69208	3225	34.62
$1/3CaHg_3 + 8/3Ca \rightarrow Ca_3Hg$	0.12	668	7662	38923	3392	37.25
$Sn + 2Ca \rightarrow Ca_2Sn$	**0.53**	**903**	**5249**	**24515**	**4216**	**31.13**

Table 2. Candidates for high performance M-Ca alloy-type anodes with restrictive voltage constraint ($V_{threshold}$ = 0.53 V). For each candidate system we show the reactant, final product, averaged voltage, gravimetric capacity, volumetric capacity, energy density, specific energy, and volume expansion maximum.

Candidates and reactions	Averaged calciation voltage (V)	Gravimetric Capacity (mAh/g)	Volumetric Capacity (mAh/mL)	Energy Density (Wh/L)	Specific Energy (Wh/kg)	Volume Expansion per Ca/Å^3
Si + Ca → CaSi	0.55	1908	4446	20673	8874	27.60
As + 2Ca → Ca_2As	0.75	1431	8271	36830	6371	30.93
Sb + 2Ca → Ca_2Sb	0.67	880	5778	26156	3985	29.66
Pd + 3/2Ca → 1/2Ca_3Pd_2	0.54	755	9070	42259	3520	33.50
Ge + Ca → CaGe	0.67	738	3932	17799	3340	26.90
Bi + 2Ca → Ca_2Bi	0.59	513	5031	23206	2366	28.37
Pt + 5/3Ca → 1/3Ca_5Pt_3	0.67	458	9825	44498	2074	29.40
Au + 5/3Ca → 1/3Ca_5Au_3	0.56	454	8795	40824	2105	34.41
Sn + 7/6Ca → 1/6Ca_7Sn_6	**0.59**	**527**	**3062**	**14109**	**2426**	**27.59**

Supplementary Materials *for*

Discovery of calcium-metal alloy anodes for reversible Ca-ion batteries

Zhenpeng Yao,[12] Vinay I. Hegde,[2] Alán Aspuru-Guzik,[1345*] Chris Wolverton[2*]

[1]*Department of Chemistry and Chemical Biology, Harvard University, 12 Oxford Street, Cambridge, Massachusetts 02138, United States*

[2]*Department of Materials Science and Engineering, Northwestern University, 2220 Campus Drive, Evanston, Illinois 60208, United States*

[3]*Department of Chemistry and Department of Computer Science, University of Toronto, Toronto, Ontario M5S 3H6, Canada*

[4]*Vector Institute for Artificial Intelligence, Toronto, Ontario M5S 1M1, Canada*

[5]*Canadian Institute for Advanced Research (CIFAR) Senior Fellow, Toronto, Ontario M5S 1M1, Canada*

**Correspondence: alan@aspuru.com **Correspondence: c-wolverton@northwestern.edu*

Table of Contents

Supplementary Table S1 2

Supplementary Table S2 5

Supplementary Table S3 7

Supplementary Table S4 10

Table S1. Full reaction pathways for candidates with relaxed voltage constraint ($V_{threshold}$ = 0.1V). For each reaction of specific candidate system, we show the reactant, product, voltage, gravimetric capacity, volumetric capacity, energy density, specific energy, and volume expansion.

Candidates and reactions	Calciation voltages (V)	Gravimetric Capacity (mAh/g)	Volumetric Capacity (mAh/mL)	Energy Density (Wh/L)	Specific Energy (Wh/kg)	Volume Expansion per Ca/Å^3
$Si + 1/2Ca \rightarrow 1/2CaSi_2$	0.58	954	2223	10261	4404	27.29
$Si + 14/19Ca \rightarrow 1/19Ca_{14}Si_{19}$	0.56	1406	3276	15193	6522	26.04
$Si + Ca \rightarrow CaSi$	0.55	1908	4446	20673	8874	27.60
$Si + 5/3Ca \rightarrow 1/3Ca_5Si_3$	0.40	3181	7410	35581	15273	52.32
$Si + 2Ca \rightarrow Ca_2Si$	0.35	3817	8892	43089	18495	31.89
$Ga + 1/4Ca \rightarrow 1/4CaGa_4$	0.91	192	1147	4919	824	23.57
$Ga + 3/8Ca \rightarrow 1/8Ca_3Ga_8$	0.83	288	1720	7520	1260	28.77
$Ga + 1/2Ca \rightarrow 1/2CaGa_2$	0.79	384	2294	10118	1695	24.71
$Ga + 3/5Ca \rightarrow 1/5Ca_3Ga_5$	0.70	461	2753	12403	2078	28.02
$Ga + 1Ca \rightarrow CaGa$	0.48	769	4589	21668	3630	33.22
$Ga + 11/7Ca \rightarrow 1/7Ca_{11}Ga_7$	0.33	1208	7211	35145	5888	35.16
$Ga + 5/3Ca \rightarrow 1/3Ca_5Ga_3$	0.31	1281	7648	37397	6265	36.08
$Ga + 28/11Ca \rightarrow 1/11Ca_{28}Ga_{11}$	0.22	1957	11680	58178	9746	36.12
$Al + 1/4Ca \rightarrow 1/4CaAl_4$	0.50	497	1322	6211	2333	37.42
$Al + 1/2Ca \rightarrow 1/2CaAl_2$	0.50	993	2644	12422	4666	31.34
$Al + 13/14Ca \rightarrow 1/14Ca_{13}Al_{14}$	0.28	1845	4910	24149	9071	36.47
$Pd + 1/5Ca \rightarrow 1/5CaPd_5$	1.12	101	1209	4938	411	23.32
$Pd + 1/2Ca \rightarrow 1/2CaPd_2$	1.07	252	3023	12490	1040	26.86
$Pd + 1Ca \rightarrow CaPd$	0.69	504	6047	27284	2272	28.82
$Pd + 3/2Ca \rightarrow 1/2Ca_3Pd_2$	0.54	755	9070	42259	3520	33.50
$Pd + 5/2Ca \rightarrow 1/2Ca_5Pd_2$	0.36	1259	15117	73197	6096	36.90
$Pd + 3Ca \rightarrow Ca_3Pd$	0.30	1511	18141	88853	7400	37.75
$In + 1/2Ca \rightarrow 1/2CaIn_2$	0.68	233	1730	7825	1056	28.76
$In + 1Ca \rightarrow CaIn$	0.49	467	3460	16305	2200	31.31
$In + 2Ca \rightarrow Ca_2In$	0.29	934	6921	33973	4583	35.94
$In + 8/3Ca \rightarrow 1/3Ca_8In_3$	0.24	1245	9227	45768	6174	36.83
$In + 3Ca \rightarrow Ca_3In$	0.21	1400	10381	51759	6982	31.89
$Ge + 1/2Ca \rightarrow 1/2CaGe_2$	0.74	369	1966	8764	1645	24.91
$Ge + 1Ca \rightarrow CaGe$	0.67	738	3932	17799	3340	26.90
$Ge + 7/6Ca \rightarrow 1/6Ca_7Ge_6$	0.51	861	4587	21504	4035	28.42
$Ge + 5/3Ca \rightarrow 1/3Ca_5Ge_3$	0.51	1230	6553	30720	5765	30.72
$Ge + 2Ca \rightarrow Ca_2Ge$	0.47	1476	7864	37195	6980	31.06
$Zn + 1/13Ca \rightarrow 1/13CaZn_{13}$	1.03	63	453	1890	263	27.77

$Zn + 1/11Ca \rightarrow 1/11CaZn_{11}$	1.02	75	535	2241	312	28.53
$Zn + 1/5Ca \rightarrow 1/5CaZn_5$	0.71	164	1178	5293	737	31.26
$Zn + 1/2Ca \rightarrow 1/2CaZn_2$	0.46	410	2945	13950	1942	34.50
$Zn + 1Ca \rightarrow CaZn$	0.26	820	5890	29125	4054	39.07
$Zn + 5/3Ca \rightarrow 1/3Ca_5Zn_3$	0.16	1366	9816	49435	6881	39.78
$As + 1/3Ca \rightarrow 1/3CaAs_3$	1.14	238	1378	5599	969	27.41
$As + 2/3Ca \rightarrow 1/3Ca_2As_3$	1.12	477	2757	11257	1947	27.25
$As + 1Ca \rightarrow CaAs$	1.10	715	4135	16947	2932	31.03
$As + 5/3Ca \rightarrow 1/3Ca_5As_3$	0.90	1192	6892	29665	5132	28.63
$As + 2Ca \rightarrow Ca_2As$	0.75	1431	8271	36830	6371	30.93
$CdCu_2 + 5Ca \rightarrow Ca_5CdCu_2$	0.16	1119	10130	51056	5637	37.14
$Cu + 1/5Ca \rightarrow 1/5CaCu_5$	0.41	169	1516	7268	809	32.14
$Cu + Ca \rightarrow CaCu$	0.16	843	7581	38192	4249	37.10
$Ag + 2/7Ca \rightarrow 1/7Ca_2Ag_7$	0.56	142	1520	7055	659	33.60
$Ag + 3/8Ca \rightarrow 1/8Ca_3Ag_8$	0.51	186	1995	9363	875	34.06
$Ag + 1/2Ca \rightarrow 1/2CaAg_2$	0.46	248	2660	12596	1177	35.68
$Ag + 1Ca \rightarrow CaAg$	0.35	497	5319	25804	2410	37.36
$Ag + 5/3Ca \rightarrow 1/3Ca_5Ag_3$	0.24	828	8866	43982	4108	38.47
$1/3CaHg_3 + 4/9Ca \rightarrow 1/9Ca_4Hg_9$	0.46	28	319	1514	132	30.07
$1/3CaHg_3 + 1/6Ca \rightarrow 1/2CaHg_2$	0.46	42	479	2270	198	31.93
$1/3CaHg_3 + 2/3Ca \rightarrow CaHg$	0.44	167	1915	9118	795	28.48
$1/3CaHg_3 + 7/6Ca \rightarrow 1/2Ca_3Hg_2$	0.27	292	3352	16526	1440	35.36
$1/3CaHg_3 + 4/3Ca \rightarrow 1/3Ca_5Hg_3$	0.24	334	3831	19009	1657	36.02
$1/3CaHg_3 + 8/3Ca \rightarrow Ca_3Hg$	0.12	668	7662	38923	3392	37.25
$Sb + 1/2Ca \rightarrow 1/2CaSb_2$	0.93	220	1444	6162	939	24.81
$Sb + 11/10Ca \rightarrow 1/10Ca_{11}Sb_{10}$	0.92	484	3178	13617	2075	28.37
$Sb + 5/3Ca \rightarrow 1/3Ca_5Sb_3$	0.80	734	4815	21190	3229	31.14
$Sb + 2Ca \rightarrow Ca_2Sb$	0.67	880	5778	26156	3985	29.66
$Au + 1/5Ca \rightarrow 1/5CaAu_5$	1.26	54	1055	4159	214	31.91
$Au + 1/2Ca \rightarrow 1/2CaAu_2$	1.08	136	2638	10870	561	32.08
$Au + 3/4Ca \rightarrow 1/4Ca_3Au_4$	0.93	204	3958	16907	872	31.14
$Au + 1Ca \rightarrow CaAu$	0.82	272	5277	23107	1192	33.32
$Au + 5/4Ca \rightarrow 1/4Ca_5Au_4$	0.70	340	6596	29688	1531	33.50
$Au + 5/3Ca \rightarrow 1/3Ca_5Au_3$	0.56	454	8795	40824	2105	34.41
$Au + 7/3Ca \rightarrow 1/3Ca_7Au_3$	0.42	635	12312	58915	3038	37.30
$Au + 5/2Ca \rightarrow 1/2Ca_5Au_2$	0.40	680	13192	63387	3269	37.35
$Au + 3Ca \rightarrow Ca_3Au$	0.33	816	15830	77078	3975	38.42
$Tl + 1/3Ca \rightarrow 1/3CaTl_3$	0.48	87	1021	4818	413	23.11
$Tl + 3/5Ca \rightarrow 1/5Ca_3Tl_5$	0.46	157	1837	8703	745	27.28

Tl + 1Ca → CaTl	0.45	262	3062	14533	1245	27.86
Tl + 3Ca → Ca_3Tl	0.15	787	9185	46373	3972	30.62
Pb + 1/3Ca → 1/3$CaPb_3$	0.67	86	989	4474	390	27.40
Pb + 1Ca → CaPb	0.53	259	2966	13846	1208	28.81
Pb + 5/3Ca → 1/3Ca_5Pb_3	0.45	431	4943	23497	2050	35.53
Pb + 2Ca → Ca_2Pb	0.43	517	5931	28321	2470	34.64
Pb + 3Ca → Ca_3Pb	0.28	776	8897	43744	3816	28.10
Cd + 1/2Ca → 1/2$CaCd_2$	0.53	238	2076	9700	1114	35.54
Cd + 1Ca → CaCd	0.37	477	4152	20035	2301	35.14
Cd + 3/2Ca → 1/2Ca_3Cd_2	0.26	715	6227	30788	3536	38.22
Pt + 1/5Ca → 1/5$CaPt_5$	1.60	55	1179	4242	198	31.66
Pt + 1/2Ca → 1/2$CaPt_2$	1.43	137	2948	11124	518	24.63
Pt + 3/2Ca → 1/2Ca_3Pt_2	0.73	412	8843	39553	1843	31.83
Pt + 5/3Ca → 1/3Ca_5Pt_3	0.67	458	9825	44498	2074	29.40
Pt + 5/2Ca → 1/2Ca_5Pt_2	0.50	687	14738	69208	3225	34.62
Sn + 1/3Ca → 1/2$CaSn_3$	**0.99**	**150**	**875**	**3682**	**633**	**7.43**
Sn + 1Ca → CaSn	**0.72**	**451**	**2624**	**11746**	**2020**	**27.51**
Sn + 7/6Ca → 1/6Ca_7Sn_6	**0.59**	**527**	**3062**	**14109**	**2426**	**27.59**
Sn + 31/20Ca → 1/20$Ca_{31}Sn_{20}$	**0.59**	**700**	**4068**	**18744**	**3224**	**28.87**
Sn + 36/23Ca → 1/23$Ca_{36}Sn_{23}$	**0.53**	**706**	**4108**	**19185**	**3300**	**27.99**
Sn + 2Ca → Ca_2Sn	**0.53**	**903**	**5249**	**24515**	**4216**	**31.13**

Table S2. Full reaction pathways for candidates with restrictive voltage constraint ($V_{threshold}$ = 0.53V). For each reaction of specific candidate system, we show the reactant, product, voltage, gravimetric capacity, volumetric capacity, energy density, specific energy, and volume expansion.

Candidates and reactions	Calciation voltages (V)	Gravimetric Capacity (mAh/g)	Volumetric Capacity (mAh/mL)	Energy Density (Wh/L)	Specific Energy (Wh/kg)	Volume Expansion per Ca/Å^3
$Si + 1/2Ca \rightarrow 1/2CaSi_2$	0.58	954	2223	10261	4404	27.29
$Si + 14/19Ca \rightarrow 1/19Ca_{14}Si_{19}$	0.56	1406	3276	15193	6522	26.04
$Si + Ca \rightarrow CaSi$	0.55	1908	4446	20673	8874	27.60
$As + 1/3Ca \rightarrow 1/3CaAs_3$	1.14	238	1378	5599	969	27.41
$As + 2/3Ca \rightarrow 1/3Ca_2As_3$	1.12	477	2757	11257	1947	27.25
$As + 1Ca \rightarrow CaAs$	1.10	715	4135	16947	2932	31.03
$As + 5/3Ca \rightarrow 1/3Ca_5As_3$	0.90	1192	6892	29665	5132	28.63
$As + 2Ca \rightarrow Ca_2As$	0.75	1431	8271	36830	6371	30.93
$Sb + 1/2Ca \rightarrow 1/2CaSb_2$	0.93	220	1444	6162	939	24.81
$Sb + 11/10Ca \rightarrow 1/10Ca_{11}Sb_{10}$	0.92	484	3178	13617	2075	28.37
$Sb + 5/3Ca \rightarrow 1/3Ca_5Sb_3$	0.80	734	4815	21190	3229	31.14
$Sb + 2Ca \rightarrow Ca_2Sb$	0.67	880	5778	26156	3985	29.66
$Pd + 1/5Ca \rightarrow 1/5CaPd_5$	1.12	101	1209	4938	411	23.32
$Pd + 1/2Ca \rightarrow 1/2CaPd_2$	1.07	252	3023	12490	1040	26.86
$Pd + 1Ca \rightarrow CaPd$	0.69	504	6047	27284	2272	28.82
$Pd + 3/2Ca \rightarrow 1/2Ca_3Pd_2$	0.54	755	9070	42259	3520	33.50
$Ge + 1/2Ca \rightarrow 1/2CaGe_2$	0.74	369	1966	8764	1645	24.91
$Ge + 1Ca \rightarrow CaGe$	0.67	738	3932	17799	3340	26.90
$Bi + 11/10Ca \rightarrow 1/10Ca_{11}Bi_{10}$	0.79	282	2767	12199	1244	28.21
$Bi + 5/3Ca \rightarrow 1/3Ca_5Bi_3$	0.68	427	4192	18932	1930	30.61
$Bi + 2Ca \rightarrow Ca_2Bi$	0.59	513	5031	23206	2366	28.37
$Pt + 1/5Ca \rightarrow 1/5CaPt_5$	1.60	55	1179	4242	198	31.66
$Pt + 1/2Ca \rightarrow 1/2CaPt_2$	1.43	137	2948	11124	518	24.63
$Pt + 3/2Ca \rightarrow 1/2Ca_3Pt_2$	0.73	412	8843	39553	1843	31.83
$Pt + 5/3Ca \rightarrow 1/3Ca_5Pt_3$	0.67	458	9825	44498	2074	29.40
$Au + 1/5Ca \rightarrow 1/5CaAu_5$	1.26	54	1055	4159	214	31.91
$Au + 1/2Ca \rightarrow 1/2CaAu_2$	1.08	136	2638	10870	561	32.08
$Au + 3/4Ca \rightarrow 1/4Ca_3Au_4$	0.93	204	3958	16907	872	31.14
$Au + 1Ca \rightarrow CaAu$	0.82	272	5277	23107	1192	33.32
$Au + 5/4Ca \rightarrow 1/4Ca_5Au_4$	0.70	340	6596	29688	1531	33.50
$Au + 5/3Ca \rightarrow 1/3Ca_5Au_3$	0.56	454	8795	40824	2105	34.41
$Sn + 1/3Ca \rightarrow 1/3CaSn_3$	**0.99**	**150**	**875**	**3682**	**633**	**7.43**
$Sn + 1Ca \rightarrow CaSn$	**0.72**	**451**	**2624**	**11746**	**2020**	**27.51**

$Sn + 7/6Ca \rightarrow 1/6Ca_7Sn_6$	**0.59**	**527**	**3062**	**14109**	**2426**	**27.59**

Table S3. Non-candidate compounds with relaxed voltage constraint ($V_{threshold}$ = 0.1V). For each reaction compound system, we show the reactant, product, voltage, gravimetric capacity, volumetric capacity, energy density, specific energy, and volume expansion.

Candidates and reactions	Averaged calciation voltage (V)	Gravimetric Capacity (mAh/g)	Volumetric Capacity (mAh/mL)	Energy Density (Wh/L)	Specific Energy (Wh/kg)	Volume Expansion per Ca/Å^3
$Bi + 2Ca \rightarrow Ca_2Bi$	0.59	513	5031	23206	2366	28.37
$Ni + 1/2Ca \rightarrow 1/2CaNi_2$	0.27	457	4116	20276	2249	25.80
$Be+ 1/13Ca \rightarrow 1/13CaBe_{13}$	0.68	457	811	3662	2067	27.30
Te+ Ca → CaTe	1.66	420	2615	9255	1486	30.16
$Rh+ 1/2Ca \rightarrow 1/2CaRh_2$	0.63	260	3844	17550	1189	30.11
$Ir+ 1/2Ca \rightarrow 1/2CaIr_2$	0.70	139	3165	14250	628	25.57
$Mg+ 1/2Ca \rightarrow 1/2CaMg_2$	0.19	1103	1979	9918	5525	41.62
$CaAl_2Si_2 + 2Ca \rightarrow Ca_3Al_2Si_2$	0.40	713	1683	8080	3424	32.85
$Si_2Ni_3 + 3Ca \rightarrow Ca_3Si_2Ni_3$	0.23	692	4696	23352	3442	34.08
MnSi + Ca → CaMnSi	0.15	645	3885	19604	3257	33.82
SrSi + Ca → CaSrSi	0.20	463	1607	8036	2316	35.41
$GaPd + 3/2Ca \rightarrow 1/2 Ca_3Ga_2Pd_2$	0.40	456	4389	21052	2189	33.48
$SiAs_2 + 3/2Ca \rightarrow 1/2Ca_3Si_2As_4$	1.17	452	1785	7198	1821	22.44
$CaAl_2Ge_2 + 2Ca \rightarrow Ca_3Al_2Ge_2$	0.43	448	1631	7771	2134	32.86
LiSn + Ca → CaLiSn	0.52	417	2186	10225	1951	33.71
$CdAs_2 + 2Ca \rightarrow Ca_2CdAs_2$	1.12	409	2320	9466	1667	25.76
NiGe + Ca → CaNiGe	0.53	408	3251	15182	1905	31.14
AlPd + Ca → CaAlPd	0.20	402	3037	15170	2006	33.82
SiPd + Ca → CaSiPd	0.65	398	2985	13572	1811	28.93
CuAs + Ca → CaCuAs	1.24	387	2775	10982	1531	27.52
$SiNi_2 + Ca \rightarrow CaSiNi_2$	0.25	368	2711	13418	1823	34.64
$GeAs_2 + 3/2Ca \rightarrow 1/2Ca_3Ge_2As_4$	1.11	361	1749	7151	1477	24.01
SrGe + Ca → CaSrGe	0.29	334	1524	7488	1642	34.07
RbAs + Ca → CaRbAs	0.86	334	1233	5357	1451	34.49
$InPd_2 + 2Ca \rightarrow Ca_2InPd_2$	0.53	327	3535	16499	1526	32.89
BaSi + Ca → CaBaSi	0.19	324	1399	7004	1621	35.81
$GaNi +3/4Ca \rightarrow 1/4Ca_3Ga_4Ni_4$	0.37	313	1797	8680	1512	17.96
$SiNi + 1/2Ca \rightarrow 1/2CaSi_2Ni_2$	0.59	309	1838	8465	1422	28.32
$CoSi + 1/2Ca \rightarrow 1/2CaCo_2Si_2$	0.30	308	2058	10077	1508	35.80

$CuSn + Ca \rightarrow CaCuSn$	0.67	294	2326	10532	1331	28.35
$NiGe_2 + Ca \rightarrow CaNiGe_2$	0.76	263	1937	8595	1165	28.31
$SrSn + Ca \rightarrow CaSrSn$	0.33	260	1274	6203	1264	35.06
$RbSb + Ca \rightarrow CaRbSb$	0.77	259	993	4398	1145	34.79
$BaGe + Ca \rightarrow CaBaGe$	0.27	255	1329	6546	1257	34.36
$LiPb + Ca \rightarrow CaLiPb$	0.43	250	2004	9565	1194	32.63
$LiBi + Ca \rightarrow CaLiBi$	0.82	248	1885	8254	1086	30.49
$InRh + Ca \rightarrow CaInRh$	0.40	246	2613	12551	1182	32.40
$InPd + Ca \rightarrow CaInPd$	0.58	242	2480	11465	1120	32.79
$AlPt + Ca \rightarrow CaAlPt$	0.42	241	3000	14336	1153	31.31
$SiPt + Ca \rightarrow CaSiPt$	0.81	240	2908	12767	1054	34.14
$AlAu + Ca \rightarrow CaAlAu$	0.65	239	2547	11597	1089	29.85
$SnPd + Ca \rightarrow CaSnPd$	0.69	238	2270	10232	1073	29.27
$1/2CaZn_2Si_2 + 1/2Ca \rightarrow CaZnSi$	0.62	236	974	4458	1080	35.31
$InAu_3 + 3Ca \rightarrow Ca_3InAu_3$	0.81	228	3568	15645	999	32.94
$Kbi + Ca \rightarrow CaKBi$	0.68	216	1051	4752	977	39.95
$BaSn + Ca \rightarrow CaBaSn$	0.31	209	1112	5441	1024	34.67
$MnAs + 1/2Ca \rightarrow 1/2CaMn_2As_2$	0.83	206	1567	6848	902	39.53
$FeAs + 1/2Ca \rightarrow 1/2CaFe_2As_2$	0.94	205	1663	7078	872	28.69
$CoGe + 1/2Ca \rightarrow 1/2CaCo_2Ge_2$	0.77	204	1669	7400	903	28.12
$GaAu + Ca \rightarrow CaGaAu$	0.85	201	2417	10501	873	28.54
$NiAs + 1/2Ca \rightarrow 1/2CaNi_2As_2$	1.09	200	1544	6350	825	25.36
$CoAs + 1/2Ca \rightarrow 1/2CaCo_2As_2$	0.94	200	1665	7089	852	28.51
$GePt + Ca \rightarrow CaGePt$	0.88	200	2653	11451	864	26.42
$GePt + Ca \rightarrow CaGePt$	0.91	200	2653	11383	859	26.42
$CuBi + Ca \rightarrow CaCuBi$	0.76	197	1988	8832	873	29.12
$Si_3Ir + Ca \rightarrow CaSi_3Ir$	0.74	194	1398	6237	865	24.41
$ZnAs + 1/2Ca \rightarrow 1/2CaZn_2As_2$	1.34	191	1118	4320	738	26.24
$GaAs + 1/2Ca \rightarrow 1/2CaGa_2As_2$	0.91	185	942	4043	795	23.26
$In_2Cu + Ca \rightarrow CaIn_2Cu$	0.65	183	1364	6204	831	24.97
$SiIr + 3/4Ca \rightarrow 1/4Ca_3Si_4Ir_4$	0.67	182	2313	10475	826	31.04
$SrPb + Ca \rightarrow CaSrPb$	0.33	182	1225	5969	885	35.52
$1/2CaMn_2Ge_2 + 1/2Ca \rightarrow CaMnGe$	0.48	181	1005	4749	857	23.21
$PbAu_2 + 2Ca \rightarrow Ca_2PbAu_2$	0.84	178	2722	11862	777	30.54
$CdAu + Ca \rightarrow CaCdAu$	0.78	173	2323	10274	766	33.35
$InNi_2 + 3/4Ca \rightarrow 1/4Ca_3In_4Ni_8$	0.37	173	1591	7675	835	31.90

$InPt + Ca \rightarrow CaInPt$	0.78	173	2325	10271	764	29.82
$1/2CaCu_2Ge_2 + 1/2Ca \rightarrow CaCuGe$	0.48	171	1007	4751	809	25.47
$SnAu + Ca \rightarrow CaSnAu$	0.92	170	1878	8043	727	32.55
$SbPt + Ca \rightarrow CaSbPt$	1.04	169	2105	8757	703	25.73
$Sn_2Rh + Ca \rightarrow CaSn_2Rh$	0.72	157	1480	6626	705	29.86
$Sn_2Pd + Ca \rightarrow CaSn_2Pd$	0.76	156	1339	5938	691	27.56
$GeRu + 1/2Ca \rightarrow 1/2CaGe_2Ru_2$	0.69	154	1523	6869	696	33.59
$GeRh + 1/2Ca \rightarrow 1/2CaGe_2Rh_2$	0.91	153	1439	6181	655	29.39
$AsRu + 1/2Ca \rightarrow 1/2CaAs_2Ru_2$	1.04	152	1444	6013	634	29.83
$MnSb + 1/2Ca \rightarrow 1/2CaMn_2Sb_2$	0.87	152	1102	4777	657	48.05
$Al_9Co_2 + Ca \rightarrow CaAl_9Co_2$	0.51	149	538	2523	697	41.13
$ZnSb + 1/2Ca \rightarrow 1/2CaZn_2Sb_2$	1.05	143	892	3701	594	29.94
$CdAs + 1/2Ca \rightarrow 1/2CaCd_2As_2$	0.77	143	919	4076	634	25.10
$1/2CaAs_2Pd_2 + 1/2Ca \rightarrow CaAsPd$	0.97	133	930	3935	563	36.98
$Cu_2As + 1/2Ca \rightarrow 1/2CaCu_4As_2$	1.21	133	1039	4144	529	26.82
$In_2Ir + Ca \rightarrow CaIn_2Ir$	0.66	127	1462	6637	577	30.43
$In_2Pt + Ca \rightarrow CaIn_2Pt$	0.68	126	1334	6024	570	25.07
$In_2Au + Ca \rightarrow CaIn_2Au$	0.72	126	1211	5427	563	22.33
$Sn_2Ir + Ca \rightarrow CaSn_2Ir$	0.71	125	1347	6052	560	24.48
$CdSb + 1/2Ca \rightarrow 1/2CaCd_2Sb_2$	1.08	114	756	3115	471	27.10
$Al_2Cu + 1/4Ca \rightarrow 1/4CaAl_8Cu_4$	0.63	114	465	2128	521	9.13
$BaSn_3 + Ca \rightarrow CaBaSn_3$	0.59	109	692	3192	501	36.32
$GeIr + 1/2Ca \rightarrow 1/2CaGe_2Ir_2$	1.03	101	1392	5805	422	27.94
$In_3Au_{10} + 4Ca \rightarrow Ca_4In_3Au_{10}$	1.14	93	1475	5987	376	30.35
$CaGaPt + 1/2Ca \rightarrow 1/2Ca_3Ga_2Pt_2$	0.24	88	731	3626	436	36.35
$Bi_2Pd + 3/4Ca \rightarrow 1/4Ca_3Bi_8Pd_4$	0.85	77	868	3775	333	28.58
$1/2Ca_5Ga_2As_6 + 1/2Ca \rightarrow Ca_3GaAs_3$	0.91	68	282	1209	291	31.65
$1/2Ca_5Al_2Sb_3 + 1/2Ca \rightarrow Ca_3AlSb_3$	0.82	54	231	1011	238	34.48

Table S4. Non-candidate compounds with restrictive voltage constraint ($V_{threshold}$ = 0.53 V).

For each compound system we show the reactant, final product, averaged voltage, gravimetric capacity, volumetric capacity, energy density, specific energy, and volume expansion maximum.

Candidates and reactions	Averaged calciation voltage (V)	Gravimetric Capacity (mAh/g)	Volumetric Capacity (mAh/mL)	Energy Density (Wh/L)	Specific Energy (Wh/kg)	Volume Expansion per Ca/Å^3
$InPd_2 + 2Ca \rightarrow Ca_2InPd_2$	0.53	327	3535	16499	1526	32.89
$InAu_3 + 3Ca \rightarrow Ca_3InAu_3$	0.81	228	3568	15645	999	32.94
$NiGe + Ca \rightarrow CaNiGe$	0.53	408	3251	15182	1905	31.14
$SiPd + Ca \rightarrow CaSiPd$	0.65	398	2985	13572	1811	28.93
$SiPt + Ca \rightarrow CaSiPt$	0.81	240	2908	12767	1054	34.14
$PbAu_2 + 2Ca \rightarrow Ca_2PbAu_2$	0.84	178	2722	11862	777	30.54
$AlAu + Ca \rightarrow CaAlAu$	0.65	239	2547	11597	1089	29.85
$InPd + Ca \rightarrow CaInPd$	0.58	242	2480	11465	1120	32.79
$GePt + Ca \rightarrow CaGePt$	0.88	200	2653	11451	864	26.42
$GePt + Ca \rightarrow CaGePt$	0.91	200	2653	11383	859	26.42
$CuAs + Ca \rightarrow CaCuAs$	1.24	387	2775	10982	1531	27.52
$CuSn + Ca \rightarrow CaCuSn$	0.67	294	2326	10532	1331	28.35
$GaAu + Ca \rightarrow CaGaAu$	0.85	201	2417	10501	873	28.54
$SiIr + 3/4Ca \rightarrow 1/4Ca_3Si_4Ir_4$	0.67	182	2313	10475	826	31.04
$CdAu + Ca \rightarrow CaCdAu$	0.78	173	2323	10274	766	33.35
$InPt + Ca \rightarrow CaInPt$	0.78	173	2325	10271	764	29.82
$SnPd + Ca \rightarrow CaSnPd$	0.69	238	2270	10232	1073	29.27
$CdAs_2 + 2Ca \rightarrow Ca_2CdAs_2$	1.12	409	2320	9466	1667	25.76
$CuBi + Ca \rightarrow CaCuBi$	0.76	197	1988	8832	873	29.12
$SbPt + Ca \rightarrow CaSbPt$	1.04	169	2105	8757	703	25.73
$NiGe_2 + Ca \rightarrow CaNiGe_2$	0.76	263	1937	8595	1165	28.31
$SiNi + 1/2Ca \rightarrow 1/2CaSi_2Ni_2$	0.59	309	1838	8465	1422	28.32
$LiBi + Ca \rightarrow CaLiBi$	0.82	248	1885	8254	1086	30.49
$SnAu + Ca \rightarrow CaSnAu$	0.92	170	1878	8043	727	32.55
$CoGe + 1/2Ca \rightarrow 1/2CaCo_2Ge_2$	0.77	204	1669	7400	903	28.12
$SiAs_2 + 3/2Ca \rightarrow 1/2Ca_3Si_2As_4$	1.17	452	1785	7198	1821	22.44
$GeAs_2 + 3/2Ca \rightarrow 1/2Ca_3Ge_2As_4$	1.11	361	1749	7151	1477	24.01
$CoAs + 1/2Ca \rightarrow 1/2CaCo_2As_2$	0.94	200	1665	7089	852	28.51
$FeAs + 1/2Ca \rightarrow 1/2CaFe_2As_2$	0.94	205	1663	7078	872	28.69

$GeRu + 1/2Ca \rightarrow 1/2CaGe_2Ru_2$	0.69	154	1523	6869	696	33.59
$MnAs + 1/2Ca \rightarrow 1/2CaMn_2As_2$	0.83	206	1567	6848	902	39.53
$In_2Ir + Ca \rightarrow CaIn_2Ir$	0.66	127	1462	6637	577	30.43
$Sn_2Rh + Ca \rightarrow CaSn_2Rh$	0.72	157	1480	6626	705	29.86
$NiAs + 1/2Ca \rightarrow 1/2CaNi_2As_2$	1.09	200	1544	6350	825	25.36
$Si_3Ir + Ca \rightarrow CaSi_3Ir$	0.74	194	1398	6237	865	24.41
$In_2Cu + Ca \rightarrow CaIn_2Cu$	0.65	183	1364	6204	831	24.97
$GeRh + 1/2Ca \rightarrow 1/2CaGe_2Rh_2$	0.91	153	1439	6181	655	29.39
$Sn_2Ir + Ca \rightarrow CaSn_2Ir$	0.71	125	1347	6052	560	24.48
$In_2Pt + Ca \rightarrow CaIn_2Pt$	0.68	126	1334	6024	570	25.07
$AsRu + 1/2Ca \rightarrow 1/2CaAs_2Ru_2$	1.04	152	1444	6013	634	29.83
$In_3Au_{10} + 4Ca \rightarrow Ca_4In_3Au_{10}$	1.14	93	1475	5987	376	30.35
$Sn_2Pd + Ca \rightarrow CaSn_2Pd$	0.76	156	1339	5938	691	27.56
$GeIr + 1/2Ca \rightarrow 1/2CaGe_2Ir_2$	1.03	101	1392	5805	422	27.94
$In_2Au + Ca \rightarrow CaIn_2Au$	0.72	126	1211	5427	563	22.33
$RbAs + Ca \rightarrow CaRbAs$	0.86	334	1233	5357	1451	34.49
$MnSb + 1/2Ca \rightarrow 1/2CaMn_2Sb_2$	0.87	152	1102	4777	657	48.05
$KBi + Ca \rightarrow CaKBi$	0.68	216	1051	4752	977	39.95
$1/2CaZn_2Si_2 + 1/2Ca \rightarrow CaZnSi$	0.62	236	974	4458	1080	35.31
$RbSb + Ca \rightarrow CaRbSb$	0.77	259	993	4398	1145	34.79
$ZnAs + 1/2Ca \rightarrow 1/2CaZn_2As_2$	1.34	191	1118	4320	738	26.24
$Cu_2As + 1/2Ca \rightarrow 1/2CaCu_4As_2$	1.21	133	1039	4144	529	26.82
$CdAs + 1/2Ca \rightarrow 1/2CaCd_2As_2$	0.77	143	919	4076	634	25.10
$GaAs + 1/2Ca \rightarrow 1/2CaGa_2As_2$	0.91	185	942	4043	795	23.26
$1/2CaAs_2Pd_2 + 1/2Ca \rightarrow CaAsPd$	0.97	133	930	3935	563	36.98
$Bi_2Pd + 3/4Ca \rightarrow 1/4Ca_3Bi_8Pd_4$	0.85	77	868	3775	333	28.58
$ZnSb + 1/2Ca \rightarrow 1/2CaZn_2Sb_2$	1.05	143	892	3701	594	29.94
$BaSn_3 + Ca \rightarrow CaBaSn_3$	0.59	109	692	3192	501	36.32
$CdSb + 1/2Ca \rightarrow 1/2CaCd_2Sb_2$	1.08	114	756	3115	471	27.10
$1/2Ca_5Ga_2As_6 + 1/2Ca \rightarrow Ca_3GaAs_3$	0.91	68	282	1209	291	31.65
$1/2Ca_5Al_2Sb_6 + 1/2Ca \rightarrow Ca_3AlSb_3$	0.82	54	231	1011	238	34.48